

GPS-IDS: An Anomaly-based GPS Spoofing Attack Detection Framework for Autonomous Vehicles

Murad Mehrab Abrar, Amal Youssef, Raian Islam, Shalaka Satam, Banafsheh Saber Latibari, Salim Hariri, Sicong Shao, Soheil Salehi, and Pratik Satam

Abstract—Autonomous Vehicles (AVs) heavily rely on sensors and communication networks like Global Positioning System (GPS) to navigate autonomously. Prior research has indicated that networks like GPS are vulnerable to cyber-attacks such as spoofing and jamming, thus posing serious risks like navigation errors and system failures. These threats are expected to intensify with the widespread deployment of AVs, making it crucial to detect and mitigate such attacks. This paper proposes GPS Intrusion Detection System, or GPS-IDS, an Anomaly-based intrusion detection framework to detect GPS spoofing attacks on AVs. The framework uses a novel physics-based vehicle behavior model where a GPS navigation model is integrated into the conventional dynamic bicycle model for accurate AV behavior representation. Temporal features derived from this behavior model are analyzed using machine learning to detect normal and abnormal navigation behaviors. The performance of the GPS-IDS framework is evaluated on the AV-GPS-Dataset—a GPS security dataset for AVs comprising real-world data collected using an AV testbed, and simulated data representing urban traffic environments. To the best of our knowledge, this dataset is the first of its kind and has been publicly released for the global research community to address such security challenges.

Index Terms—Autonomous Vehicles, Anomaly Detection, CARLA, GPS Spoofing, Intrusion Detection System, Physics-based Behavior Modeling, Robotics, Secure Navigation.

I. INTRODUCTION

VEHICLES are getting increasingly autonomous and becoming ever more reliant on onboard sensors and communication networks, aiming to make transportation faster, safer, and environmentally sustainable by reducing human intervention in driving tasks [1], [75]. Researchers have shown human error to be the cause of over 90% accidents, resulting in 40 thousand deaths and over 2 million injuries annually in the United States alone [2], [3] — a statistic that will be reduced with the transition to AVs [4]. AVs rely on *Automotive Sensing*, a collection of diverse sensors that enable environmental perception and safe navigation without requiring constant human input [5]. Automotive sensing is broadly categorized into three types: *Self-sensing*, *Surrounding-sensing*, and *Localization* [5]. *Self-sensing* refers to how an autonomous vehicle gathers and interprets information about its own state, including its position, velocity, and acceleration. *Surrounding-sensing* is the ability of a vehicle to perceive its environment, like

This work is partly supported by National Science Foundation (NSF) research projects NSF-1624668, (NSF) OIA-2218046, (NSF) FAIN-1921485 (Scholarship-for-Service), NSF-2213634, Department of Energy/National Nuclear Security Administration under Award Number DE-NA0003946, AGILITY project 4263090 sponsored by KIAT (South Korea), and the University of Arizona's Research, Innovation & Impact (RII) award for the "Future Factory".

recognizing traffic signs, understanding weather conditions, or measuring the state of other vehicles around it. *Localization* integrates internal self-sensing and surrounding sensing data with external information from satellite-based navigation systems to determine the local and global positions of the vehicle. For self-sensing and surrounding sensing, AVs use an array of sensors like Inertial Measurement Units (IMUs), gyroscopes, odometers, Controller Area Network (CAN) bus, cameras, Light Detection and Ranging (LiDARs), etc. [6]. For localization and navigation, they rely on satellite-based navigation systems like Global Navigation Satellite System (GNSS) [7].

GNSSs like GPS (United States), GLONASS (Russia) [35], BeiDou (China) [36], and Galileo (European Union) [37], provide geolocation and time information to a receiver anywhere on or near the Earth. Being the pioneering system, GPS utilizes a 24-satellite constellation to provide its users with highly precise and accurate location and time information for navigation [38]. GPS offers two distinct variants: a secure military-grade GPS that is exclusively accessible to the United States military branches and a civilian GPS that is available for public use [39]. Most autonomous systems, including autonomous vehicles, robots, and drones, rely on the latter variant for navigational purposes. This heavy reliance on civilian GPS raises significant concerns due to the absence of encryption or authentication mechanisms, unlike the military-grade GPS [40]. Researchers have demonstrated that civilian GPS is vulnerable to jamming and spoofing attacks, and commercially available off-the-shelf GPS receivers lack the capability to detect and counteract such attacks [38], [40]–[42]. Various GPS spoofing techniques, including Lift-off-delay [44], Lift-off-aligned [45], Meaconing or Replay [45], Jamming and Spoofing [46], and Trajectory Spoofing [47], pose serious threats to the integrity of GPS. Such spoofing attacks can result in navigational errors, potential vehicle hijacking, or fatal collisions.

Motivated by these challenges, this paper presents GPS-IDS, an Anomaly-based Intrusion Detection System that uses a novel physics-based vehicle behavior model (a modification of the conventional dynamic bicycle model) and machine learning to detect GPS spoofing attacks on AVs. The bicycle model is a simplified representation of a vehicle's dynamics, typically used in the context of autonomous vehicle control systems. It approximates the vehicle as a two-wheel system, capturing the essential dynamics without the complexity of a full multi-wheel model. By extracting temporal features from this model, GPS-IDS captures the normal behavior of AVs.

Machine learning models are then utilized to differentiate between normal and abnormal behaviors. The detection of GPS spoofing attacks is achieved by identifying deviations from the normal behavior pattern, indicating potential intrusions.

The main contributions of this paper are as follows:

- The paper presents the *Autonomous Vehicle Behavior Model*—a hybrid vehicle model that integrates a modified physics-based dynamic bicycle model with GPS navigation. This modification allows for an accurate representation of the normal navigation behavior of AVs. Temporal features extracted from the physics-based model are utilized in the data-centric analysis to detect abnormal behaviors using machine learning.
- The paper introduces the *AV-GPS-Dataset*, including:
 - *Real-world Data*: Collected from field experiments with real GPS spoofing attacks on an AV testbed, capturing 44 features of GPS-guided navigation.
 - *Simulation-generated Data*: Generated using the CARLA (Car Learning to Act) [65] simulator, representing various urban scenarios with diverse traffic conditions. This part of the dataset helps to understand GPS spoofing effects in urban environments.
- In contrast to the existing related datasets collected solely from simulated environments [8], [10], [11], the AV-GPS-Dataset features both real-world and simulated data, providing normal and GPS spoofing attack scenarios.
- The GPS-IDS framework is evaluated using the AV-GPS-Dataset. The framework achieves:
 - An F1 score of up to 94.4%, with a 56.5% improvement in detection time compared to the existing EKF-based GPS/INS detector in real-world data.
 - An F1 score of up to 97.1% in simulation-generated data with urban traffic scenarios, demonstrating high effectiveness in diverse environments.

The rest of the paper is organized as follows: Section II discusses the background and related work; Section III introduces the GPS-IDS framework and explains the components; Section IV explains the attacker model and defines the problem statement, Section V presents the experimental evaluation of the GPS-IDS framework along with the dataset details, and Section VI concludes the paper and outlines future directions.

II. BACKGROUND AND RELATED WORK

This section outlines the relevant technical background on vehicle modeling techniques, various types of Intrusion Detection Systems, existing works on cyber-attacks and GNSS security for vehicles, and our motivations to address the current limitations.

A. Vehicle Models

1) *Physics-based Model*: A physics-based vehicle model is a mathematical representation that simulates the vehicle's physical behavior using factors like kinematics, dynamics, motion, forces, and environmental interactions. In [15], the

authors adopted a physics-based dynamic vehicle model incorporating an EKF estimator to determine the vehicle's longitudinal and lateral velocities and yaw rate. In [30], Kong et al. explored two physics-based vehicle models, namely kinematic and dynamic bicycle models, for model-based controller design in autonomous driving and presented a comparison using experimental data. Several research contributions have employed software tools such as Modelica, Robot Operating System (ROS), Gazebo, and Simulink to simulate physics-based vehicle models or their components. [16], [9], [17].

2) *Data-centric Model*: A data-centric vehicle model uses data-driven techniques and machine learning algorithms to represent the vehicle system. The model analyzes a large volume of data from sensors and sources to determine the vehicle's actions. In [18] the authors proposed a data-driven modeling approach based on Deep Neural Networks (DNNs) to compute and predict the dynamic characteristics of a vehicle. In [19], a data-driven system identification and control method is proposed for autonomous vehicles, where several vehicle dynamic variables are measured and corresponding data is collected to model a physical vehicle. In [20], the authors conducted a comparative analysis between physical and data-driven vehicle models under real-world driving conditions.

B. Intrusion Detection System (IDS)

Intrusion Detection Systems (IDS) are software designed to detect cyber-attacks and can be classified into four types [12]: 1) Signature-based IDS, 2) Anomaly-based IDS, 3) Specification-based IDS, and 4) Hybrid IDS. Signature-based IDSs rely on a pre-learned attack signature database, where each observation matched with an entry in the attack database is considered as an attack. Signature-based IDSs heavily rely on an up-to-date attack signature database and are unable to detect new or modified attacks [13]. An Anomaly-based IDS relies on modeling techniques to capture the system's normal behavior, wherein any observed behavior outside the model-defined norm is classified as malicious. This reliance on normal behavior models allows Anomaly-based IDSs to detect new or modified attacks at the cost of increased modeling complexity [14]. Specification-based IDSs use a set of rules and policies that define the expected behavior of different system components such as sensor nodes or motor commands. Hybrid IDSs are a combination of Signature-based, Anomaly-based, and Specification-based IDSs. The Anomaly-based IDS approach presented in this work detects GPS spoofing attacks on AVs by utilizing an extensive physics-based AV behavior model and real-life vehicular data, aiming to use a more accurate operational baseline and overcome the high error rates present in Anomaly-based IDSs.

C. Cyber-attacks on Vehicles

The increasing deployment of AVs increases the cyber-attack surfaces within the vehicle system that can be potentially exploited. In [56], Hoppe et al. exploited vulnerabilities present in the CAN-bus of a vehicle to attack the windows, lights, and airbags. Similarly, Miller et al. [57] successfully attacked a Jeep Cherokee 2014 by reprogramming a gateway

chip in the head unit of the vehicle. The attack enabled the vehicle to send arbitrary CAN messages, allowing access to different critical subsystems like braking and steering [58]. Similar attacks have been demonstrated against Toyota Prius 2010 and Ford Escape 2010 [61], by targeting different vehicular Electronic Control Units (ECU) and head units [60]. Similar to the CAN bus attacks, researchers have successfully targeted navigation systems in AVs like the GPS receiver [21], leading to hijacking attacks.

D. GNSS Security

In this section, we highlight the research aimed at detecting GNSS attacks. GNSS security literature can be classified into two broad categories: (1) GPS signal characteristics-based approach [21], [22], [23], [24], [25], [26], and (2) Machine learning-based approach [70], [74] [71], [10], [72], [73]. The GPS signal characteristics-based approaches rely on signal processing techniques to detect attacks. For instance, in [21], Psiaki and Humphreys proposed a GPS spoofing attack detection scheme based on the direction-of-arrival (DOA) induction. He et al. [23] proposed the use of GPS signal distortion to detect GPS spoofing attacks. For connected and autonomous vehicles, an anomaly detection model is proposed by Yang et al. [24] to detect GPS spoofing on the localization system using the “Learning From Demonstration” technique. Milaat and Liu [25] proposed a decentralized technique where vehicles exchange GPS code pseudo-range values with neighbors using short-range communications to detect high correlations during spoofed GPS signal arrival. On the other hand, machine learning-based approaches rely on machine learning and data analytics techniques to detect attacks. Researchers have used one-class classifiers [10], Artificial Neural Networks [70], Long Short Term Memory (LSTM) networks [71], [72] to detect GPS attacks.

The majority of these works adopt a segregated approach focused on sensor node-specific detection techniques and either use a small (and restrictive) GPS dataset or an attack dataset collected solely from simulated environments using tools like Matlab and Gazebo, lacking the representation of the real world. This paper overcomes these limitations by: (1) Introducing an approach that is evaluated on both real-world data including practical GPS spoofing scenarios, as well as simulated data in diverse urban environment conditions, and (2) Employing a hybrid vehicle behavior model, a combination of physics-based and data-centric models, to accurately represent the behavior of AVs. The physics-based component is a modified dynamic bicycle model that includes GPS navigation, and the data-centric component extracts temporal features from this model to model the vehicle’s normal navigation behavior and identify the deviations using machine learning — thereby detecting GPS attacks.

Unlike the traditional GNSS security approaches, our approach benefits from diverse data and the combination of both physics-based and data-centric models, giving the IDS a comprehensive view and allowing faster detection of anomalies like GPS attacks.

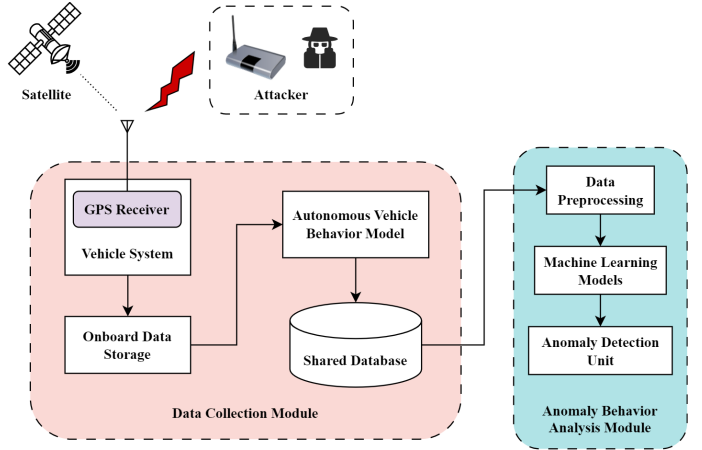


Fig. 1: GPS-IDS Architecture

III. GPS INTRUSION DETECTION SYSTEM (GPS-IDS)

GPS-IDS is an Anomaly-based Intrusion Detection System designed to identify GPS spoofing attacks on AVs by continuously monitoring the behavior of the vehicle and considering any deviation from the expected behavior as anomalous. The framework relies on a hybrid vehicle model called the *Autonomous Vehicle Behavior Model* to represent the vehicle’s behavior using both physics-based and data-centric components at any instantaneous time t . Features highlighted in the physics-based component are used in machine learning analysis to detect anomalous behavior of the vehicle. Fig. 1 shows the architecture of the GPS-IDS framework. The framework has two modules: the *Data Collection Module*, and the *Anomaly Behavior Analysis Module*.

A. Data Collection Module

This module collects the raw data from the AV system and stores it in a shared database. It ensures that the necessary data is collected in real-time and is available for subsequent analysis. It has 3 main components: 1) Vehicle System, 2) Onboard Data Storage, and 3) Autonomous Vehicle Behavior Model.

1) *Vehicle System and GPS Receiver*: The vehicle system includes a GPS receiver that is susceptible to spoofing attacks, where an attacker can manipulate the GPS receiver to provide false location data to the vehicle.

2) *Onboard Data Storage*: The onboard data storage system of the vehicle temporarily stores the raw data collected by the vehicle system. Raw data includes GPS signals and an ongoing stream of vehicle dynamics data, which are obtained from the onboard state-measuring sensors. This storage acts as a buffer that holds data before being analyzed by the subsequent modules.

3) *Autonomous Vehicle Behavior Model*: In order to establish a comprehensive behavior model of AVs, it is essential to consider four key components: (a) Localization or Navigation, (b) State Estimation, (c) Motion Planning, and (d) Control [28]— and the Autonomous Vehicle Behavior Model is comprised of these four components. Localization relies on a combination of internal and external sensors (like GPS,

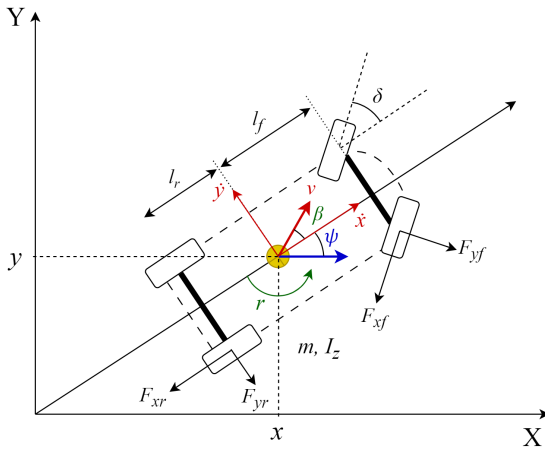


Fig. 2: Dynamic bicycle model of an autonomous vehicle in a 2-dimensional inertial frame

IMUs, Cameras, LiDARs, etc.) to collect information about the surrounding environment. The remaining three components require a mathematical representation of the vehicle that encompasses its dynamics. This study focuses specifically on GPS-guided localization in AVs, aiming to investigate the impact of a spoofing attack on the vehicle's dynamics and motion. Therefore, predicting the dynamic state of the vehicle becomes crucial. To achieve this, a simple 2 Degrees of Freedom (2 DOF) dynamic bicycle model proposed by Rajamani et al. [29] is employed. Fig. 2 depicts the dynamic bicycle model of a vehicle in a 2-dimensional inertial frame.

a) *Dynamic Bicycle Model*: The dynamic bicycle model is a simplified representation of a vehicle's dynamics and considers the effects of external forces and yaw moments acting on the vehicle, which results in an accurate calculation of dynamic parameters [29]. In a dynamic bicycle model, the inertial position coordinates and the orientation of the vehicle are defined as follows [30]:

$$v_x = \dot{x} = v \cos(\psi + \beta) \quad (1)$$

$$v_y = \dot{y} = v \sin(\psi + \beta) \quad (2)$$

$$r = \dot{\psi} = \frac{v}{l_r} \sin \beta \quad (3)$$

where x and y are the coordinates of the center of mass of the vehicle in frame (X, Y); v_x and v_y represent the longitudinal and lateral velocities of the vehicle, respectively; ψ is the yaw angle, which is the orientation of the vehicle with respect to the x-axis; r is the yaw rate or the rate of change of the yaw angle; β is the angle of the current velocity of the center of mass with respect to the longitudinal axis of the vehicle; δ is the controlled steering angle of the front wheels; and l_f and l_r are the distances of the front and the rear wheel axles from the center of mass, respectively. The differential equations associated with the dynamic bicycle model are:

$$\ddot{x} = \dot{\psi} \dot{y} + a_x \quad (4)$$

$$\ddot{y} = -\dot{\psi} \dot{x} + \frac{2}{m} (F_{yf} \cos \delta + F_{yr}) \quad (5)$$

$$\dot{r} = \ddot{\psi} = \frac{2}{I_z} (l_f F_{yf} - l_r F_{yr}) \quad (6)$$

where \dot{x} and \dot{y} denote the longitudinal and lateral velocities of the vehicle, respectively; a_x is the acceleration of the center of the mass; $\dot{\psi}$ or r is the yaw rate; m and I_z denote the vehicle's mass and yaw inertia, respectively; and F_{yf} and F_{yr} denote the lateral tire forces at the front and rear wheels of the vehicle, respectively. From the dynamic bicycle model, Newton-Euler's equations of motion are defined as follows:

$$\begin{bmatrix} F_x \\ F_y \end{bmatrix} = m \begin{bmatrix} \dot{v}_x - \dot{\psi} v_y \\ \dot{v}_y - \dot{\psi} v_x \end{bmatrix} = \begin{bmatrix} -F_{xf} \cos \delta - F_{yf} \sin \delta - F_{xr} \\ F_{yf} \cos \delta - F_{xf} \sin \delta + F_{yr} \end{bmatrix} \quad (7)$$

$$\tau = I_z \ddot{\psi} = I_z \dot{r} = l_f (F_{yf} \cos \delta - F_{xf} \sin \delta) - l_r F_{yr} \quad (8)$$

These dynamics can be simplified by disregarding the aerodynamic resistance and setting the longitudinal tire forces, F_{xf} and F_{xr} , to zero. The lateral tire forces, F_{yf} and F_{yr} are calculated by using a linear tire model, which simplifies the nonlinear characteristics of tire dynamics by establishing a linear relationship between the tire slip angles and the resulting tire forces. Considering that, F_{yf} and F_{yr} are defined as [31]:

$$F_{yf} = -C_{yf} \alpha_f \quad (9) \quad F_{yr} = -C_{yr} \alpha_r \quad (10)$$

where C_{yf} and C_{yr} are the cornering stiffness coefficients, and α_f and α_r are the slip angles of the front and rear wheels, respectively. Assuming small slip angles, we obtain [31]:

$$\alpha_f = \frac{v_y + l_f r}{v_x} - \delta \quad (11) \quad \alpha_r = \frac{v_y - l_r r}{v_x} \quad (12)$$

Finally, a simplified 2 DOF non-linear state space representation of the lateral dynamics of the vehicle can be expressed as follows [62], [63]:

$$\begin{bmatrix} \dot{v}_y \\ \dot{r} \end{bmatrix} = \begin{bmatrix} \mathbf{a}_{11} & \mathbf{a}_{12} \\ \mathbf{a}_{21} & \mathbf{a}_{22} \end{bmatrix} \begin{bmatrix} v_y \\ r \end{bmatrix} + \begin{bmatrix} \mathbf{b}_{11} \\ \mathbf{b}_{21} \end{bmatrix} \delta \quad (13)$$

where,

$$\mathbf{a}_{11} = \frac{C_{yf} + C_{yr}}{m v_x} \quad \mathbf{a}_{12} = \frac{l_f C_{yf} - l_r C_{yr}}{m v_x^2}$$

$$\mathbf{a}_{21} = \frac{l_f C_{yf} - l_r C_{yr}}{I_z} \quad \mathbf{a}_{22} = \frac{l_f^2 C_{yf} - l_r^2 C_{yr}}{I_z v_x}$$

$$\mathbf{b}_{11} = -\frac{C_{yf}}{m v_x} \quad \mathbf{b}_{21} = -\frac{l_f C_{yf}}{I_z}$$

In the state space model of equation 13, the input is the steering angle δ and the states are the lateral velocity v_y and yaw rate r .

b) *Localization/ Navigation*: The GPS enables the vehicle to determine its position and localize to the destination. Since this paper focuses on presenting a GPS intrusion detection system, only GPS-based navigation is considered, and camera or vision sensor-based perception is not taken into account. To ensure safe GPS-guided localization for autonomous vehicles, it is necessary to continuously monitor various parameters such as GPS latitude and longitude, signal quality, GPS Dilution of Precision (DOP), and the number of

satellites the vehicle is locked with. The normal behavior of the GPS signal for vehicular localization can be modeled by constantly monitoring the following parameters:

$$s_{gps}(t) = (lat, lon, dop, sat_{lock}, sat_{count})^t \quad (14)$$

where $s_{gps}(t)$ is the incoming GPS signal from satellites at time t ; lat and lon are the GPS latitude and longitude at t , respectively; dop denotes the Dilution of Precision (DOP) or the quality of the incoming GPS signal at t ; and sat_{lock} and sat_{count} respectively denote the number of satellites the vehicle is locked with and the number of available satellites at t . It is noteworthy that the current GPS-guided localization behavior model only considers positional parameters and signal strength, excluding the analysis of physical layer parameters of GPS signal due to existing research on such GPS attack detectors, as outlined in section II-D.

c) *State Estimation*: One of the well-established solutions for estimating the state of nonlinear systems is the Extended Kalman Filter or EKF. It integrates measurements from multiple sensors with a system model to estimate the state of the system with improved accuracy [53]. In the context of a GPS-guided AV, the EKF utilizes multiple sensor measurements in conjunction with the dynamic vehicle model to make accurate estimation about the vehicle's state, including its position, orientation, velocity, etc. This estimation procedure takes into account the nonlinear relationship between the measurements and the position, while also considering measurement noise. EKF state estimator with GPS/INS fusion is capable of detecting sensor anomalies and attacks against autonomous vehicles by monitoring the measurement deviations of multi-sensor readings [48], [55]. A similar GPS/INS fusion using EKF dynamic state estimator has been employed in our vehicle model and experimental testbed. In Section V, it is shown that the GPS-IDS approach is able to detect a GPS spoofing attack faster than the employed EKF-based GPS/INS detection approach, which is supported by experimental validation.

For ease of description, we can rewrite equation 13 in the following forms:

$$\left. \begin{array}{l} \dot{\mathbf{x}}(t) = f_{state}(\mathbf{x}(t), u(t)) \\ \dot{\mathbf{x}} = \mathbf{a}\mathbf{x} + \mathbf{b}u \end{array} \right\} \quad (15)$$

where vehicle state $\mathbf{x} = [v_y \ r]^t$, control input $u = [\delta]^t$, and f_{state} is the nonlinear function reproducing equation 13. According to the dynamic bicycle model, the normal behavior of the vehicle's lateral dynamics is characterized by the state parameters, v_y and r , and the steering angle δ . In conjunction with the lateral dynamics model, the EKF allows us to fuse and compare multiple state-measuring sensor readings to estimate the vehicle's state with improved accuracy. To incorporate an EKF-based estimation, the vehicle can be described as a discrete time-varying system in the following forms:

$$\mathbf{x}_{k+1} = f_{cd}(\mathbf{x}_k, u_k, W_k) \quad (16)$$

$$\mathbf{y}_{k+1} = g_{cd}(\mathbf{x}_k, E_k) \quad (17)$$

where f_{cd} is the prediction equation; \mathbf{x}_k and u_k are the state and the input at the k^{th} time, respectively; W_k is the prediction noise; g_{cd} is the observation equation; and E_k

denotes the observation noise. The Jacobian matrix of the nonlinear prediction and observation equation are defined as:

$$F = \left. \frac{\partial f_{cd}}{\partial \mathbf{x}} \right|_{\hat{\mathbf{x}}_{k-1}, u_k} \quad (18) \quad G = \left. \frac{\partial g_{cd}}{\partial \mathbf{x}} \right|_{\hat{\mathbf{x}}_k} \quad (19)$$

Thus, the nonlinear system can be transformed into a linear system with an update process by the following equations:

$$\mathbf{x}_{k+1} = F\mathbf{x}_k + W_k \quad (20) \quad \mathbf{y}_{k+1} = G\mathbf{x}_k + E_k \quad (21)$$

$$\mathbf{x}_{k+1|k} = F\hat{\mathbf{x}}_{k|k} + W_k \quad (22) \quad \mathbf{y}_{k+1|k} = G\hat{\mathbf{x}}_{k|k} + E_k \quad (23)$$

The final EKF estimated value can be obtained by:

$$\hat{\mathbf{x}}_{k+1|k+1} = \mathbf{x}_{k+1|k} + \mathbf{K}_{k+1|k}(\mathbf{y}_{k+1} - \mathbf{y}_{k+1|k}) \quad (24)$$

d) *Motion Planning*: The vehicle plans a safe and efficient path to follow from its current position (x, y) to the target destination (x_t, y_t) . It uses GPS to determine its current position and generates a continuous sequence of target yaw angles, $\psi_t(t)$ and cross-track errors, $e(t)$ to guide itself to the desired path. The cross-track error refers to the perpendicular distance of the vehicle from the current position to the desired path. Algorithm 1 outlines the target yaw angle calculation process from GPS coordinates [32].

Algorithm 1 Target Yaw Calculation from GPS Coordinates

```

1: Function TargetYawFromGPS (current_latitude,
   current_longitude, target_latitude, target_longitude)
2: while (TargetYawFromGPS = True) do
3:    $\Delta$  longitude  $\leftarrow$  target_longitude - current_longitude
4:    $p = \sin(\Delta \text{ longitude}) \times \cos(\text{target\_latitude})$ 
5:    $q = \cos(\text{current\_latitude}) \times \sin(\text{target\_latitude})$ 
       $- \sin(\text{current\_latitude}) \times \cos(\text{target\_latitude})$ 
       $\times \cos(\Delta \text{ longitude})$ 
6:    $\psi_t = \arctan(p, q)$  [ $\psi_t$  = target yaw angle]
7:   return  $\psi_t$ 
8: end while

```

From the calculated target yaw, $\psi_t(t)$ and current yaw, $\psi(t)$, the motion planning algorithm can calculate the instantaneous cross-track error, $e(t)$ using the following relationship:

$$e(t) \propto \sin(\psi_t(t) - \psi(t)) \quad (25)$$

From 25, we can say that when the vehicle is traveling along the desired path, $\psi(t) = \psi_t(t)$, and $e(t) = 0$. When the vehicle deviates from the desired path, $\psi(t)$ differs from $\psi_t(t)$ and the $e(t)$ increases accordingly. In general, an increase in the difference between the target yaw angle and the current yaw angle leads to a corresponding amplification in the cross-track error.

e) *Controller*: The vehicle requires a control algorithm to mitigate the cross-track error and navigate safely. There are different types of controllers depending on vehicle-specific models and computational resources, such as Model Predictive Controller (MPC), Fuzzy Logic Controller, Proportional-Integral-Differential (PID) Controller, etc. In this study, we

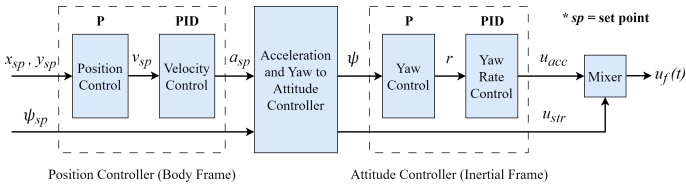


Fig. 3: PID Cascade Control Architecture

focus on the PID controller as it is one of the most widely used control algorithms and easy to implement on testbeds.

The PID controller is typically used for controlling the *Position* (e.g. latitude and longitude) and *Attitude* (e.g. yaw/heading angle) of an AV. The controller continuously adjusts the steering and acceleration control signals to minimize the cross-track error. According to the proportional (P), integral (I), and derivative (D) terms of $e(t)$, the control signal $u_c(t)$ is obtained, which is formulated as follows:

$$u_c(t) = K_p e(t) + K_i \int_0^t e(t) dt + K_d \frac{de(t)}{dt} \quad (26)$$

where K_p , K_i , and K_d are the Proportional, Integral, and Differential gain coefficients, respectively. The term $e(t)$ denotes the present cross-track error, $\int_0^t e(t) dt$ denotes the accumulated cross-track error over time, represented as the definite integral of $e(t)$ with respect to time, and $\frac{de(t)}{dt}$ is the change in cross-track error with respect to time, represented as the derivative of $e(t)$ with respect to time. The final control signal $u_f(t)$ will be comprised of an acceleration component and a steering angle component, which can be expressed as:

$$u_f(t) = u_{acc}(t) + u_{str}(t) = K_{acc}a(t) + K_{str}\delta(t) \quad (27)$$

where $u_{acc}(t)$ and $u_{str}(t)$ are the acceleration and steering control signal components, respectively. K_{acc} is the proportional gain for acceleration, K_{str} is the proportional gain for steering, and $a(t)$ and $\delta(t)$ are instantaneous acceleration and steering angle, respectively. Fig. 3 illustrates the PID cascade control architecture used to control the position and attitude of the AV model.

Derived from the discussed software elements, the architecture of the Autonomous Vehicle Behavior Model is depicted in Fig. 4. From the figure, we can observe that the model is established on 14 features—Localization/ Navigation block: Latitude (*lat*), Longitude (*lon*), Horizontal DOP (*hdop*), Vertical DOP (*vdop*), Satellite Lock (*Satlock*), Satellite Count (*Sat_{count}*); Motion Planning block: Cross-Track Error (*e*); Controller block: Steering Angle (δ); and Vehicle Dynamics block: Longitudinal Position (*x*), Lateral Position (*y*), Yaw Angle (ψ), Longitudinal Velocity (*v_x*), Lateral Velocity (*v_y*), and Yaw Rate (*r*). Data from these features are acquired by the Data-centric Component, and machine learning techniques are employed to model AV behavior and detect anomalies.

B. Anomaly Behavior Analysis (ABA) Module

Satam et al. have presented an IDS for wireless networks based on Anomaly Behavior Analysis (ABA) [13], [27], which

forms the basis of this module. However, we improved it by integrating both physics and data, rather than relying solely on data to detect GPS spoofing on AVs.

The ABA module for AVs is defined over a finite set of driving events U . Set U is partitioned into two subsets: *Normal* events N and *Abnormal* or *Attack* events A , such that $N \cup A = U$ and $N \cap A = \emptyset$. A representation map R maps events in U to patterns in U^R such that $U \xrightarrow{R} U^R$. Likewise, N^R and A^R respectively represent the events in N and A , such that $N \xrightarrow{R} N^R$, $A \xrightarrow{R} A^R$, and $N^R \cup A^R = U^R$. A detector D is defined as $D = (f_{norm}, M)$; where f_{norm} is the normal behavior characterization function expressed as $f_{norm} : U^R \times M \Rightarrow [0, 1]$ and M is the system memory that stores the normal behavior model extracted from the set of normal events N^R . Function f_{norm} specifies the degree of abnormality of a sample $s \in U^R$ by comparing it with M . The higher the value of $f_{norm}(s, M)$, the more abnormal the sample is. If the value of $f_{norm}(s, M)$ exceeds a predefined threshold \mathbb{T} , detector D raises an alarm indicating the occurrence of an abnormal or attack event. We can consider D for any sample $s \in U^R$ as:

$$D(s) = \begin{cases} \text{Abnormal} & \text{if } f_{norm}(s, M) > \mathbb{T} \\ \text{Normal} & \text{otherwise} \end{cases} \quad (28)$$

Detection occurs when detector D identifies a sample as abnormal, whether it is truly an anomaly or a normal sample misclassified as one. The detection errors are defined over a test set U_t^R which is a subset of U^R , $U_t^R \subseteq U^R$. The detector considers two kinds of errors: *False Positives* and *False Negatives*. A *False Positive* detection occurs when a normal sample $s \in N^R$ is detected as an abnormal event and is defined as $\varepsilon^+ = \{s \in N^R | D(s) = \text{abnormal}\}$, while a *False Negative* detection occurs when the detector classifies an abnormal sample $s \in A^R$ as a normal event (undetected anomalies), that is $\varepsilon^- = \{s \in A^R | D(s) = \text{normal}\}$. The objective of GPS-IDS is to tune the predefined threshold \mathbb{T} , so that the overall error is minimized. Particularly, we prioritize the minimization of *False Negative* errors, as these undetected attacks pose greater risks compared to false alarms in the context of AVs. In the GPS-IDS approach, ABA is applied using machine learning (Experiment 3: V-D3) and the threshold \mathbb{T} is tuned from optimization (Experiment 4: V-D4).

IV. ATTACKER MODEL AND PROBLEM STATEMENT

We focus on the GPS spoofing attack that interferes with the target AV by injecting a malicious GPS signal into the vehicle's GPS receiver unit. The attacker is modeled as a malicious entity capable of generating, recording, and transmitting fake GPS signals with false coordinates corresponding to any location of his choice wirelessly using a spoofer device. The attacker can be an internal entity who is inside the victim vehicle and very close to the GPS receiver, or an external entity who is moving along with the victim vehicle with a directional antenna pointed toward it and staying within a specified range. It is assumed that the attacker only knows the current location of the victim vehicle and has no knowledge about (1) the low-level control algorithm settings; (2) control commands

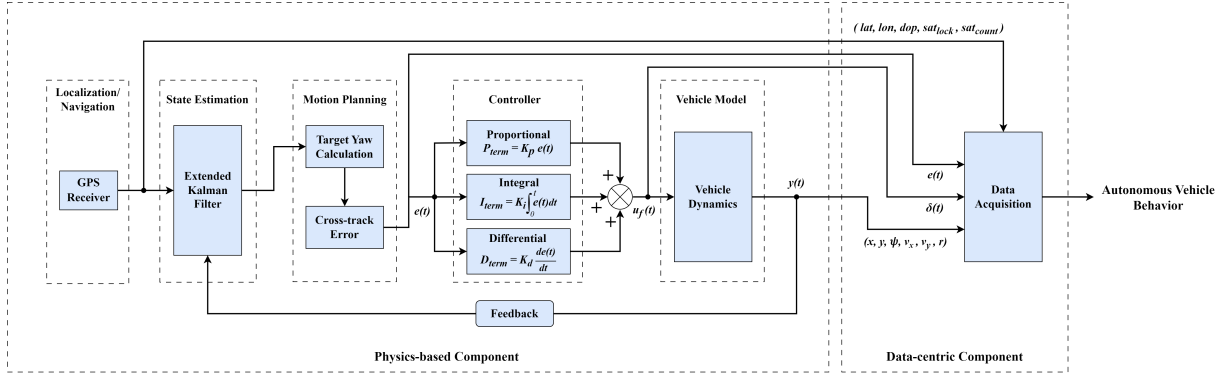


Fig. 4: Autonomous Vehicle Behavior Model

from the autonomous navigation system of the vehicle. In this study, it is shown that even though the attacker has no prior knowledge about the vehicle's control system, a GPS spoofing attack is capable of compromising the closed-loop control system and the measured states of the vehicle.

A. Mathematical model of the spoofed GPS signal

To model a spoofed GPS signal, the attacker must replicate the Radio Frequency carrier wave, the Pseudorandom noise code (PRN), and the data bits of each GPS signal that he or she intends to spoof. As stated by Psiaki and Humphreys, [33] a typical GPS signal $y(t)$ takes the following form:

$$y(t) = \mathbf{Re} \left\{ \sum_{i=1}^N A_i D_i [t - \tau_i(t)] C_i [t - \tau_i(t)] e^{j\varphi} \right\} \quad (29)$$

$$\varphi = \omega_c t - \phi_i(t) \quad (30)$$

where N is the number of individual signals transmitted by each GPS satellite. A_i , $D_i(t)$, and $C_i(t)$ correspond to the carrier amplitude, data bit stream, and spreading code (often a Binary Phase Shift Keying, BPSK-PRN code or a Binary Offset Carrier, BOC-PRN code) of the i th signal, respectively. $\tau_i(t)$ is the i th signal's code phase, ω_c is the nominal carrier frequency, and $\phi_i(t)$ is the i th beat carrier phase. The attacker sends a set of spoofed signals $y_{spf}(t)$ that are similar to as follows:

$$y_{spf}(t) = \mathbf{Re} \left\{ \sum_{i=1}^{N_{spf}} A_{i_{spf}} \hat{D}_i [t - \tau_{i_{spf}}(t)] C_i [t - \tau_{i_{spf}}(t)] e^{j\hat{\varphi}} \right\} \quad (31)$$

$$\hat{\varphi} = \omega_c t - \phi_{i_{spf}}(t) \quad (32)$$

where N_{spf} is the number of spoofed signals (typically $N_{spf} = N$). Each spoofed signal must have the same spreading code $C_i(t)$ as the corresponding true signal in order to deceive the receiver, and usually, it broadcasts its best estimate of the same data bit stream $\hat{D}_i(t)$. The spoofed amplitudes, code phases, and carrier phases are, respectively, $A_{i_{spf}}$, $\tau_{i_{spf}}(t)$, and $\phi_{i_{spf}}(t)$ for $i = 1, \dots, N_{spf}$. According to the mathematical model, when a spoofing attack is successful, the victim vehicle's GPS receiver antenna receives $y(t) + y_{spf}(t)$.

This attack is still detectable by several approaches discussed in II section. To enhance the stealthiness of our GPS spoofing attack, realistic noise was added to the generated

spoofed signals by sampling a Gaussian distribution with a large variance, as detailed by Wang et al. [67]. The addition of Gaussian noise aims to mimic the natural variations and imperfections present in genuine GPS signals, making it more challenging for IDSs to identify the spoofing attack.

Finally, the total signal received, $y_{total}(t)$ at the victim vehicle's GPS receiver antenna is:

$$y_{total}(t) = y(t) + y_{spf}(t) + \nu(t) \quad (33)$$

where $\nu(t)$ is the Gaussian noise component added to the spoofing attack to make it stealthy.

B. Mathematical model of the attack impacts on the Vehicle

If the attack is successful, the GPS receiver of the vehicle will receive incorrect location information, and the current latitude and longitude will be replaced by spoofed latitude and longitude. The function *TargetYawFromGPS()* in Algorithm 1 takes the spoofed latitude and longitude as inputs and calculates the spoofed yaw angle, $\psi_{t_{spf}}$. This means that the proportionality of equation 25 calculates a spoofed cross-track error, $e_{spf}(t)$. The PID controller takes $e_{spf}(t)$ as input and equation 26 and 27 become:

$$u_{spf}(t) = \begin{cases} K_p e_{spf}(t) + K_i \int_0^t e_{spf}(t) dt + K_d \frac{de_{spf}(t)}{dt} \\ K_{acc} a_{spf}(t) + K_{str} \delta_{spf}(t) \end{cases} \quad (34)$$

where $u_{spf}(t)$, $a_{spf}(t)$, and $\delta_{spf}(t)$ represent the spoofed control signal, spoofed acceleration, and spoofed steering angle, respectively. $u_{spf}(t)$ goes to the vehicle system as actuator command, which results in $\delta_{spf}(t)$ and the vehicle loses its control at a time instance t . The state space representation of equation 13 thus becomes:

$$\begin{bmatrix} \dot{v}_y \\ \dot{r}_{spf} \end{bmatrix} = \begin{bmatrix} \mathbf{a}_{11} & \mathbf{a}_{12} \\ \mathbf{a}_{21} & \mathbf{a}_{22} \end{bmatrix} \begin{bmatrix} v_y \\ r \end{bmatrix} + \begin{bmatrix} \mathbf{b}_{11} \\ \mathbf{b}_{21} \end{bmatrix} \delta_{spf} \quad (35)$$

where $[v_y \dot{r}_{spf}]$ is the spoofed lateral dynamic state of the vehicle. In this state, the vehicle will start to deviate from its normal lateral dynamic behavior and move toward the spoofed GPS location. Based on the discussion, the flow of the GPS spoofing attack is summarized in Algorithm 2.

Algorithm 2 GPS Spoofing Attack

Input: Spoofed signal y_{spf} , Duration of attack t_{attack} , Bias angle caused by attack ϑ , Current state \mathbf{x} , Spoofed state \mathbf{x}_{spf} , Gaussian noise component $\nu(t)$, current_latitude, current_longitude, spoofed_latitude, spoofed_longitude

Output: Attack flag \mathbf{A} , State update \mathbf{x}_{new}

- 1: Attacker sends $y_{spf} + \nu \Rightarrow$ stealthy attack
- 2: **if** receiver antenna receives $y_{total} = y + y_{spf} + \nu$ **then**
- 3: $\mathbf{A} = \text{True}$
- 4: **else**
- 5: $\mathbf{A} = \text{False}$
- 6: **while** ($t_{attack} = \text{True}$) **do**
- 7: Compute $\psi_{t_{spf}}$ using *TargetYawFromGPS*
(current_longitude, current_latitude,
spoofed_longitude, spoofed_latitude) [algorithm 1]
- 10: $\psi_{t_{spf}} \leftarrow \psi_t + \vartheta$ [update ψ_t with bias ϑ]
- 11: $e_{spf} \Rightarrow \mathbf{f}(\psi_{t_{spf}} - \psi_t)$ [using equation 25]
- 12: $u_{spf} \Rightarrow e_{spf}$ [using equation 34]
- 13: $\delta_{spf} \Rightarrow u_{spf}$
- 14: Update \mathbf{x} [using equation 15]
- 15: **end while**
- 16: **end if**

C. Problem Statement

In autonomous driving applications, GPS spoofing attacks involve the deliberate manipulation of GPS signals to deceive the vehicle's onboard navigation system, which can cause the vehicle to deviate from its intended path, leading to accidents or even hijacking. To ensure the safety of passengers and pedestrians, attacks must be detected in a timely manner. Based on the above discussions, the GPS intrusion detection problem investigated in this paper can be stated as follows:

Let us consider an AV modeled by Fig. 4, that has a state space representation described by equation 13 under normal conditions and equation 35 under the influence of a GPS spoofing attack. Assuming the vehicle is under normal operating conditions at the initial time, we have to design an anomaly-based intrusion detection strategy to detect GPS anomalies and, in turn, detect the GPS attacks.

V. EXPERIMENTAL EVALUATION

To validate the proposed GPS-IDS framework and demonstrate its effectiveness, field experiments were conducted using an AV robotic testbed. The testbed was designed and developed by following the Autonomous Vehicle Behavior Model presented in Fig. 4. This testbed was utilized to perform GPS spoofing attack experiments and collect relevant real-world data. In addition, simulated data with urban environment scenarios were generated using CARLA simulator. All the collected datasets have been used to conduct a series of experiments and validate the GPS-IDS framework.

A. Field Experiments and Data Collection

1) *Autonomous Vehicle Testbed (AVT):* The Autonomous Vehicle Testbed or AVT is a custom-built autonomous rover

that can navigate through a predefined path using GPS guidance. It utilizes an array of state-measuring sensors, including an accelerometer, magnetometer, barometer, gyroscope, and digital compass for accurate state estimation. Following the Autonomous Vehicle Behavior Model, the AVT employs a PID controller and a GPS/INS fusion-based EKF failsafe. The EKF failsafe is triggered when the EKF variances associated with any two state-measuring sensor readings exceed a predefined EKF threshold value for 1 second. The AVT uses Ardupilot [64], an open-source software and hardware platform designed for building custom unmanned ground and aerial robotic vehicles. An Ardupilot-based autopilot generates the velocity and steering angle commands from the GPS and feedback from the state-measuring sensors of the AVT. These commands are then passed to the PID controller for execution. To program the AVT and define a path to follow using GPS, a Ground Control Station software supported by Ardupilot was utilized. The Ground Control Station computer receives all vehicular data via the telemetry modules in real time and stores them in the local memory of the computer. These vehicular data are referred to as "Dataflash logs", and collected at Ardupilot's default data update rate of 1 Hz.

The hardware architecture of the AVT is divided into two parts: the Rover Unit and the Attacker Unit. The Rover Unit consists of a 1/10th scale Radio Controlled truck chassis, a Pixhawk flight controller, a Neo M8N GPS receiver with a built-in compass, telemetry modules, Radio Transmitter-Receiver modules, and other related components. The Attacker Unit consists of a Raspberry Pi-4 model B to generate the spoofed GPS baseband signal data stream. A HackRF One Software Defined Radio (SDR) converts this data stream to Radio Frequency and transmits the spoofed signal with an antenna. The hardware architecture of the AVT is presented in Fig. 5.

2) *Practical GPS Spoofing Attack on the AVT:* To perform the GPS spoofing attack on the AVT, a real-life spoofing attack scenario was generated based on the *Attacker Model* outlined in Section IV of this paper. The attack experiment utilized a single spoofed signal, mathematically denoted as $N_{spf} = 1$. Consistent with the standard L1 GPS signal, the spoofed signal employed a carrier wave frequency of 1575.42 MHz. The navigation message contained information specific to a spoofed location, which was modulated onto the carrier wave using the BPSK modulation technique. The GPS satellite constellation was specified via a GPS broadcast ephemeris file (a collection of the individual site navigation files). The sampling frequency was set to 2600 MHz and a Gaussian noise of 20 MHz centered around 1575.42 MHz was generated for a stealthy attack. The spoofed signal was generated using the GPS-SDR-SIM tool [76] and transmitted at a rate of 1 Hz.

To ensure ethical compliance and prevent interference with other GPS receivers or critical navigation systems, the transmission range and strength of the spoofed signal were strictly controlled and contained — limiting it to less than 3 meters by controlling the transmit power. A test receiver was placed at various distances to measure the range. The transmit gain was set very low (≈ -10 dB) and then gradually incremented while monitoring the spoofed signal's range. The gain setting

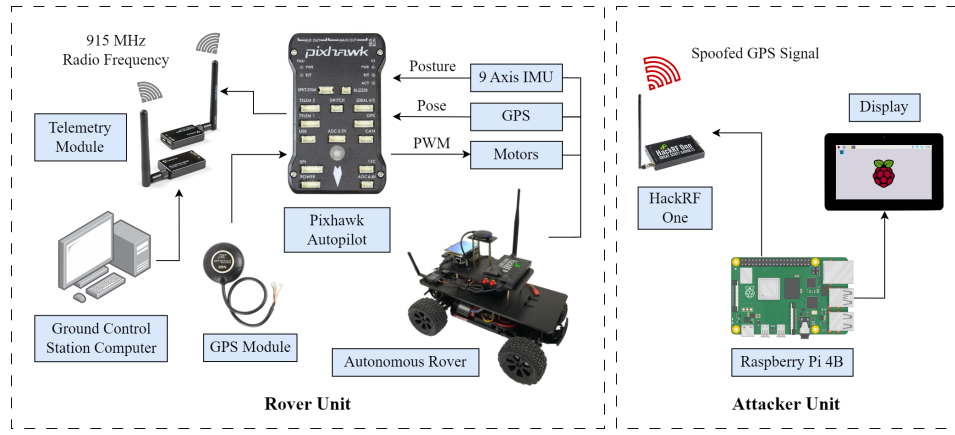


Fig. 5: Hardware Architecture of the AVT

at which the signal was detectable at 3 meters and dropped off significantly beyond that range was noted (≈ 0 dB) and utilized in the experiments. The spoofing experiments were conducted in open, wide fields with no other vehicles or critical systems within range. As outlined in Algorithm 2, the spoofing attack affected the AVT control system and compromised its normal state.

3) *Real Data Collection*: The real-world datasets were collected in two distinct locations separated by approximately 4 miles: The University of Arizona campus, and the Alvernon Park— both located in Tucson, Arizona, USA. During data collection, the vehicle was consistently operated in autonomous mode guided by GPS. As a safety precaution, a wireless remote controller was employed for manual control of the vehicle to mitigate potential hazards.

To collect normal data, a circular path consisting of 7 waypoints including the home location was mapped and uploaded to the AVT from the Ground Control Station. Each round of normal data collection was considered completed if the vehicle followed all 7 waypoints and returned to its home location. This way, 180 rounds of normal data were collected while no attack was imposed. To collect attack data, the AVT was operated in autonomous mode for 10 seconds without imposing any attack; afterward, the attack was launched. During one round of attack data collection, the spoofing attack was performed on the vehicle for 300 seconds. This way, 65 rounds of attack data were collected. By extracting the dataflash logs after each autonomous operation, all vehicular data were stored, labeled, and added to the dataset. To distinguish between the two categories of data, the normal and attack data were labeled by 0's and 1's, respectively.

B. Simulation Experiments

1) *CARLA Simulator*: CARLA is an open-source urban driving simulator designed to facilitate the development, training, and validation of autonomous driving systems. CARLA provides a highly detailed, realistic environment that mimics urban settings, complete with dynamic weather conditions, diverse vehicle and pedestrian traffic, and a wide array of sensory inputs. We utilized CARLA to run simulations in an urban environment where various vehicle sensor data was

collected, including GPS signals, accelerometer readings, and gyroscope data.

2) *Simulation Environment*: The simulations were conducted in CARLA Town01, which is a small, urban-like area featuring a mix of streets, a few T-junctions, and a variety of buildings. The town is surrounded by coniferous trees and contains several small bridges that span a river, dividing the town into two halves. We ran 3 simulations, each lasting 5 minutes, to capture various randomizations of vehicle start locations. The simulations were performed in an urban town setting with clear weather conditions. In each simulation, 100 vehicles were spawned at different locations. Among these, 10 vehicles were equipped with GPS receivers, accelerometers, and gyroscopes. All vehicles in the simulations were controlled by an autopilot system to generate subsequent locations. The sensor data from the 10 equipped vehicles were monitored and logged at 0.1-second intervals.

3) *GPS Spoofing Attack Simulation*: To simulate the GPS spoofing attack, we modified the GPS spoofed entries according to the equation: $X' \sim \mathcal{N}(X + \mu, \sigma^2)$. where X' is the GPS reading (latitude and longitude) after adding the spoofing effect, X is the GPS reading before adding the spoofing effect, μ the mean of the GPS readings for each vehicle and σ is the standard deviation of the GPS readings for each vehicle. This GPS spoofing method was used in [66]. We generated a GPS spoofed entry for each original entry.

C. Autonomous Vehicle GPS Datasets (AV-GPS-Datasets)

The AV-GPS-Datasets have two parts with a total of 6 subsets, namely *AV-GPS-Dataset (Real Data)*, with subsets 1—3, and *AV-GPS-Dataset (Simulation-generated Data)*, with subsets 4—6. Each subset contains two classes of data: Normal and Attack data, and they are extracted as Comma Separated Value (CSV) files. The AV-GPS-Datasets mainly consist of temporal features of AVs collected using the AVT and CARLA simulated environment.

1) *AV-GPS-Dataset 1—3 (Real Data)*: AV-GPS-Dataset 1 is the largest subset containing 62,042 entries, out of which, 46,787 are labeled as normal vehicular data (approximately 75%), and 15,255 are labeled as attack data (approximately 25%). This set contains experimental data from two different

locations at the University of Arizona Campus. Both locations were chosen so that the AVT could have a clear reception of the GPS signal and no obstacle could block the GPS reception. Here, we collected the normal data and attack data in separate sessions, and afterward, merged the two types of data to form the dataset. The dataset comprises three distinct GPS spoofing scenarios- **Scenario I**: GPS spoofing when the AVT is following a straight line, **Scenario II**: GPS spoofing when the AVT is making turns, and **Scenario III**: GPS spoofing when the AVT is stationary.

AV-GPS-Dataset 2 is the second subset and contains 6,890 entries, with 5,184 labeled as normal (approximately 75%) and 1,706 labeled as attack data (approximately 25%). This dataset was collected from outside the University of Arizona Campus (Alvernon Park), incorporating a different location and driving environment. This location had more trees to obstruct GPS reception partially, making the autonomous operation more challenging for the AVT. This subset was also collected in separate sessions, with normal and attack data merged to form the dataset. It comprises two spoofing scenarios, **Scenario I** and **Scenario III**.

AV-GPS-Dataset 3 is the smallest subset collected from the eastern part of the University of Arizona Campus. It contains only 636 entries, with 241 labeled as normal (approximately 38%) and 395 labeled as attack data (approximately 62%). This subset was collected in a single session to capture the transition between the normal and attack state of the AVT. The complete AV-GPS-Dataset is publicly available at [34], with a comprehensive explanation of the dataset features.

2) *AV-GPS-Dataset 4–6 (Simulation-generated Data)*: To prepare AV-GPS-Dataset 4–6 from CARLA simulations, the vehicle sensor data was first collected in normal conditions without imposing GPS spoofing attacks. Data from the 14 features highlighted in the Autonomous Vehicle Behavior Model was collected. Three simulations were conducted, resulting in three distinct datasets: AV-GPS-Dataset 4 with 29,735 entries of normal data, AV-GPS-Dataset 5 with 22,120 entries of normal data, and AV-GPS-Dataset 6 with 21,315 entries of normal data. Each dataset features different random starting positions for each vehicle. Traffic density varied across the datasets, with AV-GPS-Dataset 4 having heavy traffic density, AV-GPS-Dataset 5 having moderate traffic density, and AV-GPS-Dataset 6 having sparse traffic density. We then introduced GPS spoofing attacks by adding corresponding spoofed data entries as explained in V-B3 and reran the experiments to collect the attack data, effectively doubling the number of data points in each dataset. As a result, AV-GPS-Dataset 4 contains a total of 59,470 data points, AV-GPS-Dataset 5 contains 44,240 data points, and AV-GPS-Dataset 6 contains 42,630 data points.

D. Experimental Analysis

In this section, we present the experiments that were used to analyze the AV-GPS-Datasets and evaluate the performance of the GPS-IDS approach.

1) *Experiment 1- State Estimation of the AVT using the Autonomous Vehicle Behavior Model*: This experiment establishes a connection between the Autonomous Vehicle Behavior

TABLE I: Physical Parameters of the Autonomous Vehicle Testbed (AVT)

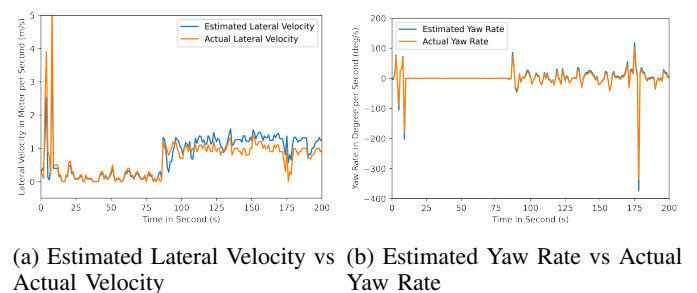
AVT Parameters	Values
Mass, m	2.5 kg
Length, l	0.56 m
Width, w	0.32 m
Yaw moment of inertia, I_z	0.0867 kg - m ²
Distance between the front wheel axle and Center of Mass, l_f	0.22 m
Distance between the rear wheel axle and Center of Mass, l_r	0.22 m
Nominal velocity, v	1 m/s

Model and the actual AVT. In this experiment, we estimated the states of the AVT using the dynamic bicycle model presented in section III-A3a. The estimated results are then compared with the actual vehicle states obtained from 46,787 instances of normal data from AV-GPS-Dataset 1. Since a small-scale testbed is used to represent the real vehicle, it is assumed that the distances of the front and the rear wheel axle from the center of mass are equal. It is also assumed that the cornering stiffness coefficients for the front and rear wheels are equal to 1. Table I presents the physical parameters of the AVT that were used to identify the system matrix “**a**” and the input matrix “**b**”. Substituting these values in Equation 13, the final dynamic state equation obtained is as follows:

$$\begin{bmatrix} \dot{v}_y \\ \dot{r} \end{bmatrix} = \begin{bmatrix} 0.8 & 0.0 \\ 0.0 & 1.1169 \end{bmatrix} \begin{bmatrix} v_y \\ r \end{bmatrix} + \begin{bmatrix} -0.4 \\ -2.5384 \end{bmatrix} \delta \quad (36)$$

The estimated results of the lateral dynamics of the AVT compared with the actual values are shown in Fig. 6. From Fig. 6, it can be observed that the estimated states using the dynamic bicycle model follow a similar distribution as the actual values of the yaw rates and lateral velocities. Therefore, the derived dynamic bicycle model can represent the lateral dynamics of the AVT well. This points out the necessity of adapting the dynamic bicycle model to capture the behavior of AVs and collect data on the parameters identified by the vehicle behavior model. Since the presented vehicle model is capable of estimating the distributions of the next states of the AVT correctly, the state space representation accurately models the testbed. The differences in these values can be accepted based on the assumption that the field experiments added some noise that is not considered in the state equation.

2) *Experiment 2- Attack Impact on Pose Measurements and Controller Input/ Output*: This experiment presents a



(a) Estimated Lateral Velocity vs Actual Lateral Velocity (b) Estimated Yaw Rate vs Actual Yaw Rate

Fig. 6: Estimated Dynamics vs Actual Dynamics

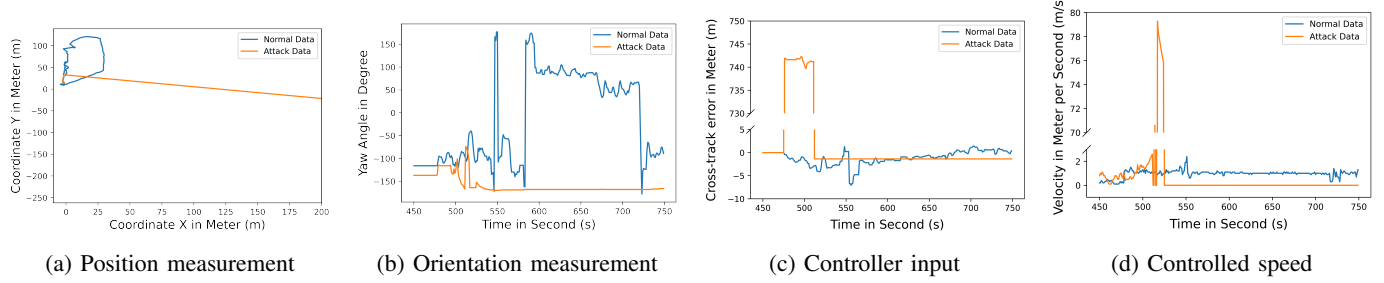


Fig. 7: AVT pose measurements and controller input/ output under the influence of GPS spoofing attack. Axis breaks are utilized to shrink down large segments and enhance readability

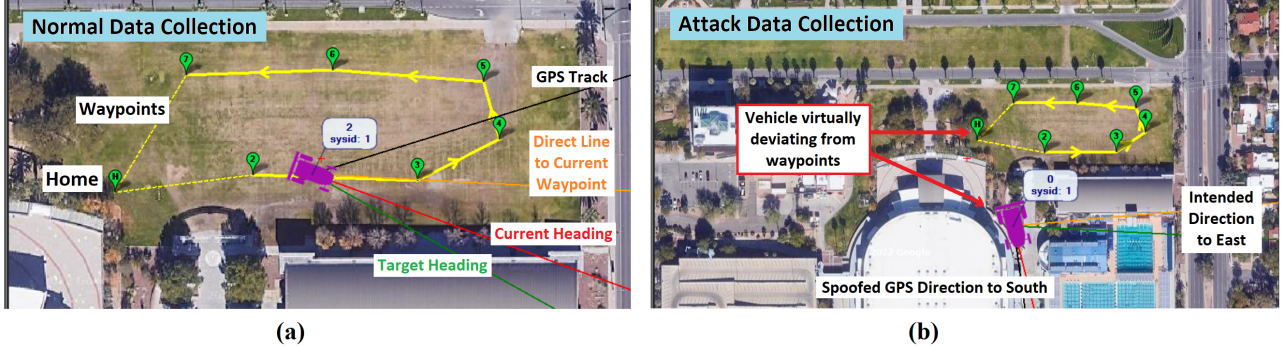


Fig. 8: Screenshot of the data collection procedure from the Ground Control Station computer. Fig. (a) AVT following given waypoints during normal data collection, Fig. (b) AVT virtually moving to spoofed GPS location during attack data collection

comprehensive analysis of the behavior of the AVT under normal operating conditions and under the influence of real GPS spoofing attack. To facilitate a clear comparison of the attack impact, we plotted one round of normal data with the corresponding attack data from AV-GPS-Dataset 1 pertaining to the pose measurements and controller input/ output of the AVT, as presented in Fig. 7. We can observe that the AVT follows a circular trajectory (7a) with a velocity ranging from 0 m/s to 2.5 m/s. During its path traversal, it effectively corrects cross-track errors and adjusts its yaw angles accordingly (7d).

It is apparent that the AVT's position is significantly affected by the spoofed GPS signals. It deviates from its regular circular trajectory and moves toward a different direction along the X coordinate (Fig. 7a) at an irregular velocity spiking to as high as 80 m/s, and then decelerating to 0 m/s (Fig. 7d). In Fig. 7c, we can observe an abnormal rise in cross-track errors exceeding 740 meters, then dropping to around 0 meters after 35 seconds and continuing to be the same. The AVT was unable to correct this error and adjust its heading, causing the yaw angle to remain unchanged (Fig. 7b). During this time, the AVT had lost all the satellite locks and remained stationary due to the variance in EKF estimates. Nonetheless, on the Ground Control Station map, the AVT was observed virtually progressing toward the location indicated by the spoofed signals, which is shown in Fig. 8.

3) *Experiment 3- Performance Analysis of the Machine Learning Models with Different Training Sets from Real Data:* This experiment evaluated the GPS-IDS approach on the AV-GPS-Dataset 1—3 using different machine learning models. To

benchmark various machine learning techniques, including ensemble methods, neural networks, and tree-based algorithms, seven models were chosen for detection: Random Forest (RF), XGBoost (XGB), Support Vector Machine Classifier (SVC), Multi-Layer Perceptron (MLP), AdaBoost, Gradient Boosting (GB), and Decision Tree (DT). The 14 features associated with the physics-based component of the Autonomous Vehicle Behavior Model (Fig. 4) are utilized in the machine learning analysis. To maintain the proportion of samples for each class consistently across both training and testing phases, stratified 5-fold sampling was employed to partition the data into training and testing sets. The training approach is based on supervised learning, where 4 folds (80%) were utilized for training, and the remaining fold (20%) was utilized for testing. Three cases were considered to train the models, **Case I:** Train on 80% of AV-GPS-Dataset 1, and test on 20% of AV-GPS-Dataset 1, AV-GPS-Dataset 2 and AV-GPS-Dataset 3; **Case II:** Train on 80% of AV-GPS-Dataset 2, and test on AV-GPS-Dataset 1, 20% of AV-GPS-Dataset 2 and AV-GPS-Dataset 3; **Case III:** Train on 80% of AV-GPS-Dataset 3, and test on AV-GPS-Dataset 1, AV-GPS-Dataset 2 and 20% of AV-GPS-Dataset 3. For all three cases, the performance of the machine learning models is measured in terms of Accuracy, Precision, Recall, and F1-score. For each model, a combination of hyperparameters was utilized and fine-tuned to find the optimal performance. The performance of machine learning algorithms on different datasets is presented in Table II. The results indicate that the performance varies across different datasets as the training set changes. It can be observed

TABLE II: Performance of the Machine Learning Classification Models on AV-GPS-Datasets 1—3 (Real Data)

	AV-GPS-Datasets 1—3	Metrics	RF	XGB	SVC	MLP	Adaboost	GB	DT	
Case I Trained with 80% of Dataset 1	Test on 20% of Dataset 1	Accuracy	0.972	0.965	0.972	0.974	0.867	0.970	0.933	
		Precision	0.994	0.969	0.985	0.979	0.671	0.962	0.810	
		Recall	0.899	0.893	0.903	0.919	0.935	0.919	0.965	
		F1 Score	0.944	0.929	0.942	0.948	0.782	0.939	0.881	
	Test on Dataset 2	Accuracy	0.975	0.979	0.999	0.995	0.250	0.842	0.861	
		Precision	0.912	0.933	0.999	0.984	0.248	0.610	0.640	
		Recall	0.997	0.986	0.997	0.996	1	1	0.997	
		F1 Score	0.953	0.959	0.998	0.990	0.397	0.758	0.780	
	Test on Dataset 3	Accuracy	0.965	0.945	0.963	0.948	0.636	0.874	0.902	
		Precision	0.997	1	0.997	0.967	0.636	0.839	0.883	
		Recall	0.948	0.913	0.945	0.950	1	0.992	0.975	
		F1 Score	0.972	0.954	0.970	0.958	0.778	0.909	0.927	
Average F1 Score in Case I			0.956	0.947	0.970	0.965	0.652	0.869	0.862	
Case II Trained with 80% of Dataset 2	Test on Dataset 1	Accuracy	0.891	0.890	0.760	0.964	0.891	0.982	0.973	
		Precision	0.992	0.994	0.980	0.996	0.992	0.978	0.997	
		Recall	0.576	0.570	0.058	0.861	0.577	0.952	0.899	
		F1 Score	0.729	0.725	0.109	0.924	0.730	0.965	0.946	
	Test on 20% of Dataset 2	Accuracy	0.998	0.998	0.998	0.996	0.974	0.970	0.922	
		Precision	0.998	0.998	0.994	0.998	0.998	0.961	0.926	
		Recall	0.996	0.996	0.995	0.985	0.897	0.919	0.753	
		F1 Score	0.997	0.997	0.997	0.992	0.945	0.939	0.830	
	Test on Dataset 3	Accuracy	0.973	0.971	0.963	0.971	0.973	0.874	0.965	
		Precision	1	1	0.997	0.997	0.997	0.839	1	
		Recall	0.958	0.955	0.945	0.958	0.960	0.992	0.945	
		F1 Score	0.978	0.977	0.970	0.977	0.978	0.909	0.972	
Average F1 Score in Case II			0.902	0.900	0.692	0.964	0.884	0.938	0.916	
Case III Trained with 80% of Dataset 3	Test on Dataset 1	Accuracy	0.891	0.891	0.760	0.903	0.739	0.766	0.888	
		Precision	0.983	0.982	0.939	0.904	0.487	0.536	0.982	
		Recall	0.581	0.582	0.061	0.693	0.546	0.586	0.570	
		F1 Score	0.730	0.731	0.115	0.784	0.515	0.560	0.721	
	Test on Dataset 2	Accuracy	0.998	0.998	0.807	0.990	0.953	0.973	0.995	
		Precision	0.995	0.993	0.979	0.961	0.842	0.903	0.985	
		Recall	1	1	0.228	1	1	1	0.998	
		F1 Score	0.997	0.996	0.369	0.980	0.914	0.949	0.991	
	Test on 20% of Dataset 3	Accuracy	0.962	0.959	0.945	0.940	0.952	0.951	0.971	
		Precision	0.984	0.965	0.967	0.946	0.963	0.953	1	
		Recall	0.955	0.970	0.945	0.960	0.963	0.970	0.955	
		F1 Score	0.969	0.968	0.956	0.953	0.963	0.962	0.977	
Average F1 Score in Case III			0.899	0.898	0.480	0.905	0.797	0.823	0.896	
Average F1 Score of all three cases			0.919	0.915	0.714	0.944	0.777	0.876	0.891	

that Case I exhibits high accuracy and F1 scores for most models, while the F1 scores drop for most models in Case III. This drop can be attributed to the smaller size of the training set in Case III, which contains a limited number of entries representing only the transition of the attack. In this case, the test sets are significantly larger than the training set (AV-GPS-Dataset 1 is over 110 times larger, and AV-GPS-Dataset 2 is over 12 times larger), which declines the model performances. Overall, MLP consistently performs with F1 scores above 90% in all three cases, achieving the highest average F1 score of 94.4%. Following closely, RF and XGB demonstrated similar and second-best performances, achieving average F1 scores of 91.9% and 91.5%, respectively, in the three considered cases. The DT classifier secured the third-best performance, attaining an average F1 score of 89.1% across the three cases.

4) Experiment 4- Tuning of the Detection Threshold \mathbb{T} :

In this experiment, we conducted an analysis to optimize the predefined detection threshold \mathbb{T} of the GPS-IDS framework by evaluating the probability scores of normal data and attack data from AV-GPS-Dataset 3. The machine learning model that performed the best in Experiment 3, namely MLP, was employed for this purpose. The resulting data were plotted to determine a suitable detection margin, as illustrated in Fig. 9.

Fig. 9 depicts the probability score distributions for normal and attack data obtained by applying Case I and Case II training methodologies on the same graph. By comparing the distributions, it becomes evident that the two kinds of data can be effectively distinguished with a significant margin indicated by the dotted bars. Table III shows the False Positive and False Negative Rates as we expand the margin. Based on the findings presented in Table III, we can see that selecting a detection threshold \mathbb{T} within a range of **0.4 to 0.5** produces optimal outcomes. This range leads to the misclassification of only 1 instance of normal data and 1 instance of attack data, resulting in a False Positive Rate of 0.0021 or 0.21% and a False Negative Rate of 0.0012 or 0.12%. Thus, it can be deduced that opting for a detection threshold \mathbb{T} in the range of 0.4 to 0.5 offers the lowest incidence of false detection and misclassification.

5) Experiment 5- Time Series Analysis of the Machine Learning Models:

In this experiment, we evaluated the effectiveness of the 4 best-performing models from Experiment 3 (MLP, RF, XGB, and DT) in detecting an attack with respect to time on AV-GPS-Dataset 3. The training phase involved training the models using Case I and Case II methodologies, followed by testing on AV-GPS-Dataset 3. The outcomes of

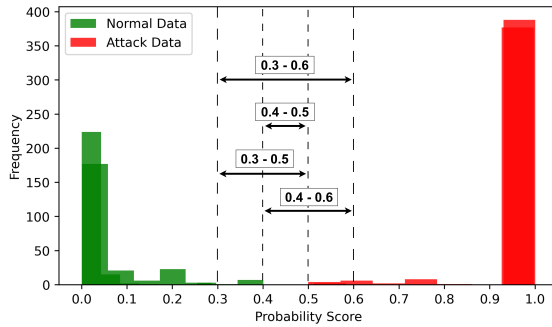


Fig. 9: Comparison of probability score distribution for normal and attack data

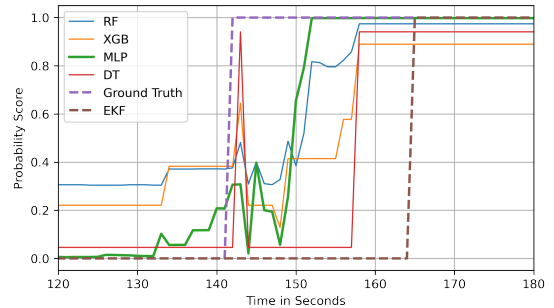
TABLE III: False Positive (FP) and False Negative (FN) Rates for Different Detection Margins in Real Datasets

Detection Margin	Normal Data Misclassified	Attack Data Misclassified	FP Rate	FN Rate
0.4 - 0.5	1	1	0.0021	0.0012
0.3 - 0.5	7	1	0.0146	0.0012
0.4 - 0.6	1	7	0.0021	0.0087
0.3 - 0.6	7	7	0.0146	0.0087

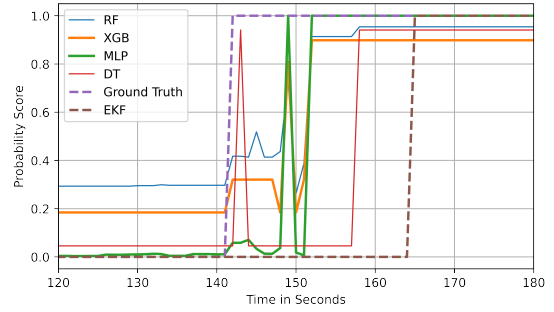
the time series analysis are represented in Fig. 10. As depicted in Fig. 10, the attack was initiated in the 142th second and was subsequently detected by the AVT's EKF algorithm in the 165th second (23 seconds delay). In both training cases, all the models succeeded in detecting the attack before the EKF. In Fig. 10a, MLP was capable of detecting the attack at the 152nd second, followed by RF, XGB, and DT at the 158th second. Similarly, in Fig. 10b, the MLP, XGB, and RF identified the attack at the 152nd second, while the DT detected it at the 158th second. Table IV summarizes the attack detection times for each classifier, revealing that MLP achieved the fastest detection time of 10 seconds in both training methodologies and showcasing a $\approx 56.5\%$ improvement in detection time compared to GPS/INS-based detection method using EKF.

While a 10-second detection delay is considerably high in AV applications, it is important to highlight that the attack requires approximately 4-7 seconds to jam the reception of the authentic GPS signal and be effective on the AV. There are scopes for further improving the detection delay by fusing multiple detection techniques and increasing granularity.

6) *Experiment 6- Performance Analysis of the Machine Learning Models with Different Simulated Training Sets:* To ensure the generalization of the GPS-IDS approach, this experiment evaluated GPS-IDS on the simulation-generated AV-GPS-Datasets 4–6 using different machine learning models. Six models were chosen: RF, XGB, SVC, MLP, AdaBoost, and GB. Similar to Experiment 3, supervised learning was utilized and stratified 5-fold sampling was employed, where 4 folds (80%) were used for training, and the remaining fold (20%) was used for testing. Three cases were considered for training, **Case IV:** Train on 80% of AV-GPS-Dataset 4, and test on 20% of AV-GPS-Dataset 4, AV-GPS-Dataset 5, and AV-GPS-Dataset 6; **Case V:** Train on 80% of AV-GPS-Dataset 5, and test on AV-GPS-Dataset 4, 20% of AV-GPS-Dataset 5 and AV-



(a) Using Case I training methodology



(b) Using Case II training methodology

Fig. 10: Time series analysis on AV-GPS-Dataset 3

TABLE IV: Results of the Time Series Analysis

	Attack Detection Time (in seconds)					
	MLP	XGB	RF	DT	EKF	Max. Improve
Case I	10	16	16	16	23	$\approx 56.52\%$
Case II	10	10	10	16	23	$\approx 56.52\%$

GPS-Dataset 6; **Case VI:** Train on 80% of AV-GPS-Dataset 6, and test on AV-GPS-Dataset 4, AV-GPS-Dataset 5, and 20% of AV-GPS-Dataset 6. For all three cases, the performance of the machine learning models is measured in terms of Accuracy, Precision, Recall, and F1-score. For each model, we used the same tuned hyperparameters utilized as Experiment 3. The performance of machine learning algorithms on different simulation generated datasets is presented in Table V. The results indicate that the performance varies across different datasets as the training set changes. MLP consistently performs with F1 scores above 93% in all three cases, achieving the highest average F1 score of 97.1%. Comparing Table II and Table V, we can see that the GPS-IDS approach demonstrates an overall better performance on the simulation-based datasets.

7) *Experiment 7- Tuning of the Detection Threshold \mathbb{T} on Simulated Data:* Similar to Experiment 4, this experiment assessed the sensitivity of the GPS-IDS detection threshold \mathbb{T} . We varied threshold values to evaluate their impacts on GPS-IDS performance using the simulation-generated datasets. The machine learning model used for this experiment was the MLP, given its consistent best performance in the previous experiments. The resulting data were plotted to determine a suitable detection margin, as illustrated in Fig. 11. By comparing the probability score distributions for normal and attack data, we again find that selecting a detection threshold \mathbb{T} within a range of 0.4 to 0.5 shows the best performance,

TABLE V: Performance of the Machine Learning Classification Models on AV-GPS-Datasets 4—6 (Simulation-generated Data)

AV-GPS-Datasets 4—6		Metrics	RF	XGB	SVC	MLP	Adaboost	GB	
Case IV Trained with 80% of Dataset 4	Test on 20% of Dataset 4	Accuracy	0.8724	0.9495	0.9091	0.9471	0.9283	0.9285	
		Precision	0.8955	0.9541	0.9093	0.9507	0.9294	0.9295	
		Recall	0.8724	0.9495	0.9091	0.9471	0.9283	0.9285	
		F1 Score	0.8705	0.9494	0.9091	0.9470	0.9283	0.9284	
	Test on Dataset 5	Accuracy	0.9494	0.9494	0.9523	0.9790	0.9486	0.9068	
		Precision	0.9541	0.9541	0.9564	0.9798	0.9534	0.9215	
		Recall	0.9494	0.9494	0.9523	0.9790	0.9486	0.9068	
		F1 Score	0.9493	0.9493	0.9522	0.9789	0.9485	0.9060	
	Test on Dataset 6	Accuracy	0.9492	0.9492	0.9527	0.9518	0.9500	0.9151	
		Precision	0.9539	0.9539	0.9568	0.9560	0.9545	0.9275	
		Recall	0.9492	0.9492	0.9527	0.9518	0.9500	0.9151	
		F1 Score	0.9491	0.9491	0.9526	0.9517	0.9499	0.9145	
Average F1 Score in Case I			0.9230	0.9493	0.9380	0.9592	0.9422	0.9163	
Case V Trained with 80% of Dataset 5	Test on Dataset 4	Accuracy	0.9409	0.9454	0.9590	0.9619	0.9040	0.9835	
		Precision	0.9471	0.9493	0.9621	0.9646	0.9040	0.9837	
		Recall	0.9409	0.9454	0.9590	0.9619	0.9040	0.9835	
		F1 Score	0.9407	0.9453	0.9589	0.9618	0.9040	0.9835	
	Test on 20% of Dataset 5	Accuracy	0.8591	0.9397	0.9492	0.9379	0.8911	0.9285	
		Precision	0.8760	0.9427	0.9538	0.9408	0.8981	0.9295	
		Recall	0.8591	0.9397	0.9492	0.9379	0.8911	0.9285	
		F1 Score	0.8575	0.9396	0.9491	0.9378	0.8906	0.9284	
	Test on Dataset 6	Accuracy	0.9461	0.9492	0.9987	0.9996	0.9635	0.9151	
		Precision	0.9513	0.9539	0.9987	0.9996	0.9660	0.9275	
		Recall	0.9461	0.9492	0.9987	0.9996	0.9635	0.9151	
		F1 Score	0.9459	0.9491	0.9987	0.9996	0.9635	0.9145	
Average F1 Score in Case II			0.9147	0.9450	0.9689	0.9664	0.9194	0.9421	
Case VI Trained with 80% of Dataset 6	Test on Dataset 4	Accuracy	0.9429	0.9400	0.9599	0.9721	0.9409	0.9511	
		Precision	0.9488	0.9430	0.9628	0.9733	0.9432	0.9554	
		Recall	0.9429	0.9400	0.9599	0.9721	0.9409	0.9511	
		F1 Score	0.9427	0.9399	0.9598	0.9721	0.9409	0.9511	
	Test on Dataset 5	Accuracy	0.9986	0.9494	0.9998	0.9997	0.9995	0.9962	
		Precision	0.9986	0.9541	0.9998	0.9997	0.9995	0.9963	
		Recall	0.9986	0.9494	0.9998	0.9997	0.9995	0.9962	
		F1 Score	0.9986	0.9493	0.9998	0.9997	0.9995	0.9962	
	Test on 20% of Dataset 6	Accuracy	0.8268	0.9090	0.9522	0.9910	0.9349	0.9107	
		Precision	0.8602	0.9229	0.9564	0.9912	0.9360	0.9214	
		Recall	0.8268	0.9090	0.9522	0.9910	0.9349	0.9107	
		F1 Score	0.8227	0.9082	0.9521	0.9910	0.9348	0.9101	
Average F1 Score in Case III			0.9213	0.9325	0.9706	0.9876	0.9584	0.9525	
Average F1 Score of all three cases			0.9197	0.9423	0.9592	0.9711	0.9400	0.9370	

TABLE VI: False Positive (FP) and False Negative (FN) Rates for Different Detection Margins in Simulated Datasets

Detection Margin	Normal Data Misclassified	Attack Data Misclassified	FP Rate	FN Rate
0.4 - 0.5	295	0	0.0076	0.0
0.3 - 0.5	764	0	0.0198	0.0
0.4 - 0.6	295	200	0.0076	0.0052
0.3 - 0.6	764	200	0.0198	0.0052

resulting in misclassification of only 295 instances of normal data and no instance of attack data and leading to a False Positive Rate of 0.0076 or 0.76% and False Negative Rate of 0%. Table. VI summarizes the different False Positive and False Negative rates for different margins in simulated data.

VI. CONCLUSION AND FUTURE WORK

This paper presents a novel anomaly behavior analysis-based GPS Intrusion Detection framework called the GPS-IDS that detects abnormal GPS navigation in AVs. The approach uses physics-based vehicle modeling to represent the behavior of the vehicle. A modified dynamic bicycle model is utilized to capture the normal behavior of the vehicle and machine learning techniques are used to detect the anomalous

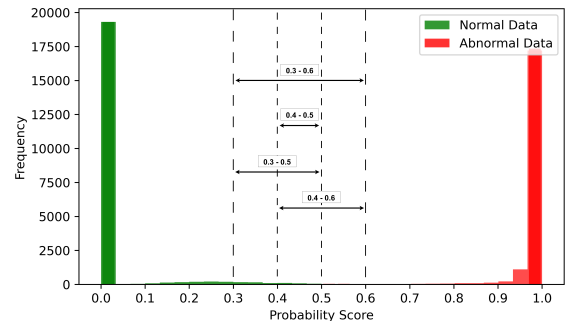


Fig. 11: Comparison of probability score distribution for normal and attack data in simulations

behavior. Moreover, a novel dataset family called the AV-GPS-Datasets with both real-world and simulated data is introduced in this paper. The performance of the proposed GPS-IDS approach is evaluated using the AV-GPS-Dataset, and the experimental results affirm its high detection rate of GPS spoofing attacks. Additionally, it is validated that the proposed approach exhibits faster detection times in comparison to the EKF-based detection algorithm in real data of AV-GPS-Datasets. In contrast to the existing segregated intrusion

detection techniques that concentrate only on individual sensor data, our approach considers the overall behavior of the system, providing a more comprehensive approach to detect GPS attacks. We argue that using GPS-IDS in conjunction with sensor-specific intrusion detection systems can provide a powerful defense mechanism against GPS spoofing attacks in autonomous vehicles. To ensure the generalization of our approach, we conducted simulation-based experiments to show that our suggested system can perform equally well in a more complex urban scenario with multiple vehicles under attack.

Moving forward, there are several promising research avenues to extend this work. The GPS-IDS algorithm can be refined by incorporating additional operational parameters in the Autonomous Vehicle Behavior Model, such as integrating accurate modeling of multiple sensors and more robust control algorithms. Further research can be done to explore the effectiveness of integrating GPS-IDS with existing sensor-specific detection systems to enhance the overall security of AVs. Additionally, GPS-IDS can be improved to detect more stealthy GPS attacks, such as dual-band spoofing and spoofing when aligned with road shapes [68], [69] against AVs. Furthermore, the feasibility of real-world deployment scenarios, including cloud environment computing, onboard deployment on resource-constrained edge devices, or hybrid computation strategies that balance cloud and onboard processing can be investigated to validate the scalability and practicality of the GPS-IDS approach. Finally, the development of a digital twin for the Autonomous Vehicle Behavior Model emerges as a promising direction, providing a virtual environment for comprehensive testing and simulation.

REFERENCES

- [1] SAE International. “Taxonomy and definitions for terms related to driving automation systems for on-road motor vehicles.” SAE International 4970.724 (2018): 1-5.
- [2] Singh, Santokh. “Critical reasons for crashes investigated in the national motor vehicle crash causation survey.” No. DOT HS 812 115. 2015.
- [3] National Highway Traffic Safety Administration. “Early Estimates of Motor Vehicle Traffic Fatalities And Fatality Rate by Sub-Categories in 2022” (2023): 1-9.
- [4] Petrović, Dorde and Mijailović, Radomir and Pešić, Dalibor. “Traffic accidents with autonomous vehicles: type of collisions, maneuvers and errors of conventional vehicles’ drivers.” Transportation Research Procedia 45 (2020): 161-168.
- [5] Van Brummelen, Jessica, et al. “Autonomous vehicle perception: The technology of today and tomorrow.” Transportation Research Part C: Emerging Technologies 89 (2018): 384-406.
- [6] Ma, Yifang, et al. “Artificial intelligence applications in the development of autonomous vehicles: A survey.” IEEE/CAA Journal of Automatica Sinica 7.2 (2020): 315-329.
- [7] Maurer, Markus, et al. Autonomous driving: technical, legal and social aspects. Springer Nature, 2016.
- [8] Rajbahadur, Gopi Krishnan, et al. “A survey of anomaly detection for connected vehicle cybersecurity and safety.” 2018 IEEE Intelligent Vehicles Symposium (IV). IEEE, 2018.
- [9] Griffin, John, John Batteh, and Johan Andreasson. “Modeling Vehicle Drivability with Modelica and the Vehicle Dynamics Library.” Proceedings of the 9th International MODELICA Conference; September 3-5; 2012; Munich; Germany. No. 076. Linköping University Electronic Press, 2012.
- [10] Whelan, Jason, et al. “Novelty-based intrusion detection of sensor attacks on unmanned aerial vehicles.” Proceedings of the 16th ACM symposium on QoS and security for wireless and mobile networks. 2020.
- [11] Whelan, Jason, et al. February 26, 2020, “UAV Attack Dataset”, IEEE Dataport, doi: <https://dx.doi.org/10.21227/00dg-0d12>.
- [12] Zarpelão, Bruno Bogaz, et al. “A survey of intrusion detection in Internet of Things.” Journal of Network and Computer Applications 84 (2017): 25-37.
- [13] Satam, Pratik, and Salim Hariri. “WIDS: An anomaly-based intrusion detection system for Wi-Fi (IEEE 802.11) protocol.” IEEE Transactions on Network and Service Management 18.1 (2020): 1077-1091.
- [14] Pacheco, Jesus, and Salim Hariri. “Anomaly behavior analysis for IoT sensors.” Transactions on Emerging Telecommunications Technologies 29.4 (2018): e3188.
- [15] Katriniok, Alexander, and Dirk Abel. “Adaptive EKF-based vehicle state estimation with online assessment of local observability.” IEEE Transactions on Control Systems Technology 24.4 (2015): 1368-1381.
- [16] Andreasson, Johan, Andreas Möller, and Martin Otter. “Modeling of a Racing Car with Modelica’s Multi-Body Library.” Workshop Proceedings. 2000.
- [17] Bhadani, Rahul Kumar, Jonathan Sprinkle, and Matthew Bunting. “The cat vehicle testbed: A simulator with hardware in the loop for autonomous vehicle applications.” arXiv preprint arXiv:1804.04347 (2018).
- [18] Pan, Yongjun, et al. “Data-driven vehicle modeling of longitudinal dynamics based on a multibody model and deep neural networks.” Measurement 180 (2021): 109541.
- [19] Fényes, Dániel, Németh, Balázs and Gáspár, Péter. “A novel data-driven modeling and control design method for autonomous vehicles.” Energies 14.2 (2021): 517.
- [20] James, Sebastian S., Sean R. Anderson, and Mauro Da Lio. “Longitudinal vehicle dynamics: A comparison of physical and data-driven models under large-scale real-world driving conditions.” Ieee Access 8 (2020): 73714-73729.
- [21] Psiaki, Mark L., Todd E. Humphreys, and Brian Stauffer. “Attackers can spoof navigation signals without our knowledge. Here’s how to fight back GPS lies.” IEEE Spectrum 53.8 (2016): 26-53.
- [22] Liang, Chen, et al. “Detection of GPS spoofing attack on unmanned aerial vehicle system.” Machine Learning for Cyber Security: Second International Conference, ML4CS 2019, Xi’an, China, September 19-21, 2019, Proceedings 2. Springer International Publishing, 2019.
- [23] He, Liang, et al. “Civilian unmanned aerial vehicle vulnerability to gps spoofing attacks.” 2014 Seventh International Symposium on Computational Intelligence and Design. Vol. 2. IEEE, 2014.
- [24] Yang, Zhen, et al. “Anomaly Detection Against GPS Spoofing Attacks on Connected and Autonomous Vehicles Using Learning From Demonstration.” IEEE Transactions on Intelligent Transportation Systems (2023).
- [25] Milaat, Fahad Ali, and Hang Liu. “Decentralized detection of GPS spoofing in vehicular ad hoc networks.” IEEE Communications Letters 22.6 (2018): 1256-1259.
- [26] Olieri, Gabriele, et al. “GPS spoofing detection via crowd-sourced information for connected vehicles.” Computer Networks 216 (2022): 109230.
- [27] Alipour, Hamid, et al. “Wireless anomaly detection based on IEEE 802.11 behavior analysis.” IEEE transactions on information forensics and security 10.10 (2015): 2158-2170.
- [28] Pendleton, Scott Drew, et al. “Perception, planning, control, and coordination for autonomous vehicles.” Machines 5.1 (2017): 6.
- [29] Rajamani, Rajesh. Vehicle dynamics and control. Springer Science & Business Media, 2011.
- [30] Kong, Jason, et al. “Kinematic and dynamic vehicle models for autonomous driving control design.” 2015 IEEE intelligent vehicles symposium (IV). IEEE, 2015.
- [31] Pepy, Romain, Alain Lambert, and Hugues Mounier. “Path planning using a dynamic vehicle model.” 2006 2nd International Conference on Information & Communication Technologies. Vol. 1. IEEE, 2006.
- [32] Mehrab Abrar, Murad, Raian Islam, and Md Abid Hasan Shanto. “An autonomous delivery robot to prevent the spread of coronavirus in product delivery system.” 2020 11th IEEE Annual Ubiquitous Computing, Electronics & Mobile Communication Conference (UEMCON). IEEE, 2020.
- [33] Psiaki, Mark L., and Todd E. Humphreys. “GNSS spoofing and detection.” Proceedings of the IEEE 104.6 (2016): 1258-1270.
- [34] AV-GPS-Dataset: Autonomous Vehicle Global Positioning System Dataset. [Online]. Available: <https://github.com/mehrab-abrar/AV-GPS-Dataset/>
- [35] Ulrichich, Yuri, et al. “GLONASS modernization.” Proceedings of the 24th International Technical Meeting of the Satellite Division of The Institute of Navigation (ION GNSS 2011). 2011.
- [36] Han, Chunhao, Yuanxi Yang, and Zhiwu Cai. “BeiDou navigation satellite system and its time scales.” Metrologia 48.4 (2011): S213.

[37] Benedicto, J., et al. "GALILEO: Satellite system design." European Space Agency. Int. Business, 2000.

[38] Tippenhauer, Nils Ole, et al. "On the requirements for successful GPS spoofing attacks." Proceedings of the 18th ACM conference on Computer and communications security. 2011.

[39] Wang, Shengqiang, et al. "Intelligent detection algorithm against uavs' gps spoofing attack." 2020 IEEE 26th International Conference on Parallel and Distributed Systems (ICPADS). IEEE, 2020.

[40] Humphreys, Todd E., et al. "Assessing the spoofing threat: Development of a portable GPS civilianspoof." Proceedings of the 21st International Technical Meeting of the Satellite Division of The Institute of Navigation (ION GNSS 2008). 2008.

[41] Shen, Junjie, et al. "Drift with devil: Security of multi-sensor fusion based localization in high-level autonomous driving under GPS spoofing." Proceedings of the 29th USENIX Conference on Security Symposium. 2020.

[42] Inside GNSS. Tesla Model S and Model 3 Prove Vulnerable to GPS Spoofing Attacks, Research from Regulus Cyber Shows. Accessed: Apr. 20, 2023. [Online]. Available: <https://insidegnss.com/tesla-models-and-model-3-prove-vulnerable-to-gps-spoofing-attacks-research-fromregulus-cyber-shows/>

[43] Haddad, Ranwa, et al. "GPS modernization and beyond." 2020 IEEE/ION Position, Location and Navigation Symposium (PLANS). IEEE, 2020.

[44] Neri, Alessandro, et al. "An anti-jamming and anti-spoofing digital beamforming platform for the GNSS-based ERTMS train control system." Proceedings of the 30th International Technical Meeting of the Satellite Division of The Institute of Navigation (ION GNSS+ 2017). 2017.

[45] Xu, Rui, et al. "Performance analysis of GNSS/INS loosely coupled integration systems under spoofing attacks." Sensors 18.12 (2018): 4108.

[46] Ranya, Eshta, and Kamal Jain. "Unmanned aerial vehicle's vulnerability to gps spoofing a review." Journal of the Indian Society of Remote Sensing 49 (2021): 585-591.

[47] Liu, Yin-Chen, Gianluca Bianchin, and Fabio Pasqualetti. "Secure trajectory planning against undetectable spoofing attacks." Automatica 112 (2020): 108655.

[48] Zhang, Dong, et al. "Cyber-attack detection for autonomous driving using vehicle dynamic state estimation." Automotive Innovation 4 (2021): 262-273.

[49] Cui, Jin, and Biao Zhang. "VERA: A simplified security risk analysis method for autonomous vehicles." IEEE Transactions on Vehicular Technology 69.10 (2020): 10494-10505.

[50] Feng, Shuo, and Simon Haykin. "Cognitive risk control for anti-jamming V2V communications in autonomous vehicle networks." IEEE Transactions on Vehicular Technology 68.10 (2019): 9920-9934.

[51] Nguyen, Van-Linh, Po-Ching Lin, and Ren-Hung Hwang. "Enhancing misbehavior detection in 5G vehicle-to-vehicle communications." IEEE Transactions on Vehicular Technology 69.9 (2020): 9417-9430.

[52] Nowdehi, Nasser, et al. "CASAD: CAN-aware stealthy-attack detection for in-vehicle networks." arXiv preprint arXiv:1909.08407 (2019).

[53] Reina, Giulio, and Arcangelo Messina. "Vehicle dynamics estimation via augmented Extended Kalman Filtering." Measurement 133 (2019): 383-395.

[54] Xu, Wenyuan, et al. "Analyzing and enhancing the security of ultrasonic sensors for autonomous vehicles." IEEE Internet of Things Journal 5.6 (2018): 5015-5029.

[55] Liu, Qipeng, et al. "Secure pose estimation for autonomous vehicles under cyber attacks." 2019 IEEE Intelligent Vehicles Symposium (IV). IEEE, 2019.

[56] Hoppe, Tobias, Stefan Kiltz, and Jana Dittmann. "Security threats to automotive CAN networks-practical examples and selected short-term countermeasures." Computer Safety, Reliability, and Security: 27th International Conference, SAFECOMP 2008 Newcastle upon Tyne, UK, September 22-25, 2008 Proceedings 27. Springer Berlin Heidelberg, 2008.

[57] Miller, Charlie, and Chris Valasek. "A survey of remote automotive attack surfaces." black hat USA 2014 (2014): 94.

[58] Miller, Charlie. "Lessons learned from hacking a car." IEEE Design & Test 36.6 (2019): 7-9.

[59] Koscher, Karl, et al. "Experimental security analysis of a modern automobile." 2010 IEEE symposium on security and privacy. IEEE, 2010.

[60] Checkoway, Stephen, et al. "Comprehensive experimental analyses of automotive attack surfaces." USENIX security symposium. Vol. 4. No. 447-462. 2011.

[61] Miller, Charlie, and Chris Valasek. "Remote exploitation of an unaltered passenger vehicle." Black Hat USA 2015.S 91 (2015): 1-91.

[62] Leung, King Tin, et al. "Road vehicle state estimation using low-cost GPS/INS." Mechanical Systems and Signal Processing 25.6 (2011): 1988-2004.

[63] Egerstedt, M., Xiaoming Hu, and A. Stotsky. "Control of a car-like robot using a virtual vehicle approach." Proceedings of the 37th IEEE Conference on Decision and Control (Cat. No. 98CH36171). Vol. 2. IEEE, 1998.

[64] ArduPilot Official Website. [Online]. Accessed: June 2022. Available: <https://ardupilot.org/>

[65] A. Dosovitskiy, G. Ros, F. Codevilla, A. Lopez, and V. Koltun, "CARLA: An Open Urban Driving Simulator," in Proceedings of the 1st Annual Conference on Robot Learning, 2017, pp. 1-16.

[66] M. Shabbir, M. Kamal, Z. Ullah, and M. M. Khan, "Securing Autonomous Vehicles Against GPS Spoofing Attacks: A Deep Learning Approach," IEEE Access, 2023.

[67] Wang, Feilong, Yuan Hong, and Xuegang Ban. "Infrastructure-enabled GPS spoofing detection and correction." IEEE Transactions on Intelligent Transportation Systems (2023).

[68] Zeng, Kexiong Curtis, et al. "All your GPS are belong to us: Towards stealthy manipulation of road navigation systems." 27th USENIX security symposium (USENIX security 18). 2018.

[69] Narain, Sashank, Aanjan Ranganathan, and Guevara Noubir. "Security of GPS/INS based on-road location tracking systems." 2019 IEEE Symposium on Security and Privacy (SP). IEEE, 2019.

[70] Manesh, Mohsen Riahi, et al. "Detection of GPS spoofing attacks on unmanned aerial systems." 2019 16th IEEE Annual Consumer Communications & Networking Conference (CCNC). IEEE, 2019.

[71] Bae, Gimin, and Inwhee Joe. "UAV anomaly detection with distributed artificial intelligence based on LSTM-AE and AE." Advanced Multimedia and Ubiquitous Engineering: MUE/FutureTech 2019 13. Springer Singapore, 2020.

[72] Agyapong, Richmond Asiedu, et al. "Efficient detection of GPS spoofing attacks on unmanned aerial vehicles using deep learning." 2021 IEEE Symposium Series on Computational Intelligence (SSCI). IEEE, 2021.

[73] Panice, G., et al. "A SVM-based detection approach for GPS spoofing attacks to UAV." 2017 23rd International Conference on Automation and Computing (ICAC). IEEE, 2017.

[74] Shafique, Arslan, Abid Mehmood, and Mourad Elhadef. "Detecting signal spoofing attack in uavs using machine learning models." IEEE access 9 (2021): 93803-93815.

[75] Satam, Shalaka. Autonomous Vehicle Security Framework (AVSF). Diss. The University of Arizona, 2022.

[76] gps-sdr-sim. GitHub Repository. [Online]. Available: <https://github.com/osqzss/gps-sdr-sim>.



Murad Mehrab Abrar is currently a Master's student in the Department of Electrical and Computer Engineering, the University of Arizona, Tucson, AZ, USA. He completed his B.Sc. in Electrical and Electronic Engineering from Ahsanullah University of Science and Technology, Dhaka, Bangladesh in 2019. His research interest focuses on robotics, autonomous vehicles, and machine learning.



Amal Youssef is currently a PhD student in the department of Electrical and Computer Engineering, Tucson, AZ, USA. She received her M.Sc. degree from the University of Utah, USA in 2018. Her current research interests include cybersecurity, autonomous vehicles, and machine learning.



Raian Islam is a Master's student in the Department of Electrical and Computer Engineering at the University of Arizona, Tucson, AZ, USA. She received her B.Sc. degree in Electrical and Electronic Engineering from Ahsanullah University of Science and Technology, Dhaka, Bangladesh, in 2019. Her current research interests include data analytics, photovoltaics, and machine learning.



Soheil Salehi (Member, IEEE) is an assistant professor in the Electrical and Computer Engineering (ECE) Department at the University of Arizona (UofA). Prior to joining the UofA, Soheil was an NSF-Sponsored Computing Innovation Fellow in the Accelerated, Secure, and Energy-Efficient Computing Laboratory and the Center for Hardware and Embedded Systems Security and Trust at the University of California, Davis (UC Davis). He received his Ph.D. and M.S. degrees in ECE from the University of Central Florida (UCF) in 2016

and 2020, respectively. He has expertise in the areas of hardware security and IoT supply-chain security as well as applied ML for secure hardware design. Moreover, he has designed novel circuits and architectures for secure and accelerated computing. He has received several nominations and award recognition, which include the Outstanding Reviewer Award at IEEE/ACM DAC'23, the Best Poster Award at ACM GLSVLSI'19, the Best Paper Award Nominee at IEEE ISQED'17 as well as the Best Presentation at UC Davis Postdoctoral Research Symposium in 2021, and the Best Graduate Teaching Assistant Award at UCF in 2016.



Shalaka Satam received her B.E. degree in Electronics and Telecommunications Engineering from the University of Mumbai in 2015. She received the M.S. and Ph.D. degrees in Electrical and Computer Engineering from the University of Arizona in 2017 and 2022, respectively. Her research focuses on cybersecurity, autonomous vehicles, and Internet of Things.



Banafsheh Saber Latibari received the B.Sc. degree in Computer Engineering from the K. N. Toosi University of Technology and the M.Sc. degree in Computer Architecture from the Sharif University of Technology. She received her Ph.D. degree from the Electrical and Computer Engineering (ECE) Department at the University of California, Davis. She is currently a Postdoctoral Research Associate at the University of Arizona's ECE Department. Her research focuses on deep learning, embedded system security, and computer architecture.



Pratik Satam is an Assistant Professor in the Department of Systems and Industrial Engineering at the University of Arizona, Tucson, AZ, USA. He is also part of the new Software Engineering program in College of Engineering at the University of Arizona. He received his B.E. degree in Electronics and Telecommunication Engineering from the University of Mumbai, in 2013, and the M.S. and Ph.D. degrees in Electrical and Computer Engineering from the University of Arizona in 2015 and 2019, respectively. From 2019 to 2022, he has been a Research Assistant Professor at the Department of Electrical and Computer Engineering, the University of Arizona. His current research interests include autonomic computing, cyber security, cyber resilience, secure critical infrastructures, and cloud security. He is an Associate Editor for the scientific journal Cluster Computing.



Salim Hariri (Senior Member, IEEE) received an M.Sc. degree from Ohio State University in 1982, and a Ph.D. degree in Computer Engineering from the University of Southern California in 1986. He is a Professor in the Department of Electrical and Computer Engineering, the University of Arizona, and the Director of the NSF Center for Cloud and Autonomic Computing (NSF-CAC). His research focuses on autonomic computing, cybersecurity, cyber resilience, and cloud security.



Sicong Shao is an assistant professor of the School of Electrical Engineering and Computer Science at the University of North Dakota (UND). Before joining UND, he was a research assistant professor in the Department of Electrical and Computer Engineering (ECE) at the University of Arizona where he also received his Ph.D. in ECE. His research interests include cybersecurity, machine learning, artificial intelligence, and software engineering.